

The Stochastic Siren: Astrophysical Gravitational-Wave Background Measurements of the Hubble Constant

Bryce Cousins,^{1,2,*} Kristen Schumacher,^{1,2} Adrian Ka-Wai Chung,^{1,2}
Colm Talbot,³ Thomas Callister,³ Daniel E. Holz,^{3,4} and Nicolás Yunes^{1,2}

¹*Department of Physics, University of Illinois Urbana-Champaign, Urbana, IL 61801, USA.*

²*Illinois Center for Advanced Studies of the Universe,
University of Illinois Urbana-Champaign, Urbana, IL 61801, USA.*

³*Kavli Institute for Cosmological Physics, The University of Chicago, Chicago, IL 60637, USA.*

⁴*Department of Physics, Department of Astronomy & Astrophysics,
Enrico Fermi Institute, University of Chicago, Chicago, IL 60637, USA.*

We report the first measurement of the Hubble constant H_0 using the stochastic gravitational-wave background arising from binary black hole mergers. This astrophysical background is sensitive to the expansion history of the Universe and thus can be used for cosmological parameter inference independently of not only electromagnetic methods, but also gravitational-wave standard siren approaches. We describe the background’s cosmological dependence and show how it can be used as a “stochastic siren” to measure H_0 . By analyzing existing resolved binary black hole mergers and the current non-detection of the background, we find that H_0 can be measured more accurately relative to using resolved mergers alone. We also note that the stochastic siren may serve a unique role in the Hubble tension in that the lower bound of the H_0 measurement would progressively increase with continued non-detection of the background.

Introduction. While it has been known for over two decades that the Universe is undergoing an accelerating expansion [1], there are significant discrepancies in the measured expansion rate. In particular, the early- [2] and late-universe [3, 4] measurements of the present-day expansion rate (the Hubble constant, H_0) are in $> 5\sigma$ conflict [3], now named the Hubble tension. Late-universe probes (e.g., type Ia supernovae and the cosmic distance ladder [5–8], gravitationally-lensed systems [9, 10], and cosmic chronometers [11]) suggest higher values of H_0 ($\sim 72\text{--}74 \text{ km s}^{-1} \text{ Mpc}^{-1}$), while early-universe probes (e.g., the cosmic microwave background [2, 12], baryon acoustic oscillations [13, 14], and the inverse distance ladder [15]) suggest lower values ($\sim 67\text{--}68 \text{ km s}^{-1} \text{ Mpc}^{-1}$).

More recently, observations of gravitational waves (GWs) from the network of LIGO [16], Virgo [17], and KAGRA [18] detectors offer unique methods to study the Hubble tension. The GW amplitude of a merger provides a direct measurement of its luminosity distance, without the need for a distance ladder, so only a measurement of the merger’s redshift is required to compute H_0 . This so-called “standard siren” approach [19, 20] can be applied via “bright” sirens, wherein an electromagnetic counterpart of the merger is identified to obtain the redshift [21–26], or via “dark” sirens whose host galaxy redshift can be inferred statistically using galaxy catalogs [19, 27–41]. Other GW methods obtain the redshift by correlating galaxy distributions with merger events [42–46] or using the tidal deformability of neutron stars [47, 48].

Furthermore, features in the mass spectrum of mergers have been utilized as “spectral sirens” to break the mass-redshift degeneracy [49–56], providing a measurement of H_0 using only GWs. The most recent spectral siren analysis from the LIGO-Virgo-KAGRA (LVK) collabo-

ration [39] measures $H_0 = 46^{+49}_{-26} \text{ km s}^{-1} \text{ Mpc}^{-1}$ (maximum a-posteriori probability and 68.3% highest density interval) using 42 binary black hole (BBH) candidates from the third GW transient catalog (GWTC-3).

Beyond detecting individual mergers, the LVK collaboration searches for the GW background (GWB) arising from unresolved signals [57–59]. The GWB is thought to be dominated by distant compact binary mergers that cannot be individually detected [58, 60–62], but it may also contain contributions from other astrophysical sources and/or early-universe phenomena [63–66]. While there has been a recent possible detection of a GWB produced from supermassive BBHs using pulsar timing arrays [67–70], the stochastic astrophysical GWB composed of stellar-mass mergers has not yet been detected [58]. However, given that this GWB is composed of individual mergers, its non-detection can already be used to probe the BBH population [58, 71, 72].

A generic GWB is characterized by Ω_{gw} , the Universe’s current energy density in GWs. For an astrophysical background, this energy density depends on both the total number of binary mergers integrated over cosmic time and the available volume over which they are distributed, the latter of which depends on the cosmic expansion. Thus, the overall strength of the astrophysical GWB is affected by the Universe’s expansion history, suggesting that it can be used to measure H_0 .

In this Letter, we propose a novel method to measure H_0 by combining the search for the GWB with population inference of individual mergers, an idea we name the “stochastic siren.” The conceptual basis of the method is as follows: a smaller value of H_0 implies larger comoving volumes in the Universe, leading to more compact object mergers for a fixed merger rate and hence a larger Ω_{gw} ,

meaning that a non-detection of the GWB can exclude lower values of H_0 . Thus, by considering the GWB during cosmological inference, H_0 could be measured more accurately. We demonstrate this by analyzing BBH data from the LVK’s first three observing runs, showing that even the current non-detection of the GWB improves measurements of H_0 relative to the spectral siren alone.

We review the dependence of the GWB energy spectrum on H_0 , construct a statistical method based on the likelihood of observing individual mergers with the GWB, and present the results of applying our method to the first three LVK observing runs [58, 73]. We conclude by discussing possible applications and extensions of the stochastic sirens approach. Throughout, we refer to the resolved BBHs as “FG” (foreground) signals and unresolved BBHs as “BG” (background) signals. We use “GWB” to refer to the stochastic astrophysical background arising from stellar-mass BBH mergers, unless otherwise noted. We assume a flat cosmology ($\Omega_k = 0$) [2] but allow other cosmological energy densities and H_0 to vary. We provide Supplemental Material [74] to explicitly show the cosmological dependence of the GWB, elaborate our full population parameter results, and provide forecasts for GWB detection in various cosmologies. *GWB dependence on H_0 .* The dimensionless GW energy density from astrophysical sources is given by [75–79]

$$\Omega_{\text{gw}} = \frac{f}{\rho_c c^3} F(\vec{\phi}, f) = \frac{f}{\rho_c c^3} \int p(\vec{\phi}) \int \mathcal{F}(\vec{\phi}, f) \frac{d\dot{N}^\circ}{dz} d\vec{\phi} dz, \quad (1)$$

for speed of light c , observer-frame GW frequency f , critical mass density of the Universe $\rho_c \equiv 3H_0^2/8\pi G$ (for gravitational constant G), and the sources’ redshift-integrated flux F . The integrated flux can be written—as above—in terms of the sources’ fluence \mathcal{F} (flux times time) and rate $\frac{d\dot{N}^\circ}{dz}$ (sources per observer-frame time per redshift interval), each of which is a function of source properties $\vec{\phi}$ with probabilities $p(\vec{\phi})$.

For compact object mergers, Eq. (1) reduces to [76–78]

$$\Omega_{\text{gw}} = \frac{8\pi G}{3c^2 H_0^3} f \int \frac{\mathcal{R}(z)}{(1+z)E(z)} \left\langle \frac{dE_{\text{gw}}}{df_s} \right\rangle_{f_s} dz, \quad (2)$$

for rate density $\mathcal{R}(z)$ (mergers per comoving volume per source-frame time) and $E(z) \equiv H(z)/H_0$ (for Hubble parameter $H(z)$). The bracketed quantity in Eq. (2) is the average energy spectrum of a single binary evaluated at the source frame frequency $f_s = f(1+z)$:

$$\left\langle \frac{dE_{\text{gw}}}{df_s} \right\rangle_{f_s} = \int d\vec{\phi} p(\vec{\phi}) \frac{dE_{\text{gw}}(\vec{\phi}, f_s)}{df_s}. \quad (3)$$

Note that there is direct dependence on H_0 in Eq. (2). This arises from Eq. (1) since $\mathcal{F} \sim H_0^{-2}$ (flux scales inversely with comoving area), canceling with $\rho_c^{-1} \sim H_0^2$, leaving $d\dot{N}^\circ \sim dV_C \sim H_0^{-3}$ for comoving volume element

dV_C . We provide a detailed derivation of Eq. (2) in [74], but qualitatively outline the cosmological dependence here as follows. The value of H_0 is inversely-proportional to the comoving distance between points in space at a given redshift (see [80] and standard texts, e.g., [81]). A higher value of H_0 indicates a smaller comoving distance, so fewer mergers would be encompassed in any given comoving volume of space under a fixed merger rate density. Therefore, a universe with a higher value of H_0 would possess fewer mergers contributing to Ω_{gw} , leading to a smaller, harder-to-detect GWB signal. The inverse is also true, meaning that ruling out higher values of Ω_{gw} would correspondingly rule out lower values of H_0 . Thus, the GWB can inform measurements of H_0 as a “stochastic siren” even if it has not yet been detected.

Likelihood construction. GW merger observations follow an inhomogeneous Poisson distribution characterized by the total observer-frame merger rate across the Universe, R , and the model hyperparameters, $\vec{\lambda}$, that affect R . Taking the fraction of these mergers that are observable as $P_{\text{det}}(\vec{\lambda})$, the likelihood of observing a catalog of foreground GW events is given by [82–84]

$$\mathcal{L}_{\text{FG}}(\{d\}|\vec{\lambda}) \propto N^{N_{\text{obs}}} e^{-NP_{\text{det}}(\vec{\lambda})} \prod_{i=1}^{N_{\text{obs}}} \mathcal{L}(d_i|\vec{\lambda}), \quad (4)$$

where $N = RT$ is the total number of mergers occurring during observing time T , and the per-event likelihood terms in the product are generally calculated by explicitly marginalizing over all possible signals assuming Gaussian detector noise. We emphasize that we use a formulation of the foreground likelihood with explicit rate dependence because the rate is also explicitly required in the background likelihood. Note that while P_{det} can introduce inconsistencies in population inference [85, 86], this can be mitigated by evaluating P_{det} empirically via a synthetic injection catalog analysis, as is performed by standard analysis software such as ICAROGW [87].

Searches for an astrophysical GWB typically assume that the background is stationary, Gaussian, unpolarized, and isotropic, although see [88, 89] for alternative approaches. Such a GWB can be searched for by cross-correlating the strain measured by different pairs of detectors within the LVK network. Following [75] and [79], for a baseline comprising the detectors I and J , we define the following cross-correlation statistic,

$$\hat{C}(f) = \frac{1}{\Delta t} \frac{20\pi^2}{3H_0^2} f^3 \tilde{s}_I(f) \tilde{s}_J^*(f), \quad (5)$$

where $\tilde{s}_I(f)$ and $\tilde{s}_J(f)$ are respectively the short-time Fourier transform of the strain measured by the detectors I and J , and Δt is the segment time length. The background likelihood (\mathcal{L}_{BG}) of observing this cross-correlation statistic for the background given some $\vec{\lambda}$ is

well approximated by a Gaussian [71, 90, 91]:

$$\mathcal{L}_{\text{BG}}(\hat{C}|\vec{\lambda}) \propto \exp \left[-\frac{1}{2} \left(\hat{C} - \gamma_{\Omega_{\text{gw}}}(\vec{\lambda}) | \hat{C} - \gamma_{\Omega_{\text{gw}}}(\vec{\lambda}) \right) \right], \quad (6)$$

where $\gamma(f)$ is the overlap reduction function that gives the sensitivity of a particular pair of detectors to an isotropic background based on their relative geometry [75, 92, 93]. The inner product in this likelihood is defined as

$$(A|B) = 2T \left(\frac{3H_0^2}{10\pi^2} \right)^2 \int_0^\infty df \frac{\tilde{A}(f)\tilde{B}^*(f)}{f^6 P_I(f)P_J(f)}, \quad (7)$$

with $P_I(f)$ the one-sided noise power spectral density of detector I . Note that this likelihood depends on H_0 through the inner product, the cross-correlation statistic, and the energy density of the GWB.

Following [71], we assume the foreground and background data are independent. In practice, there is some cross-contamination due to the observed mergers contributing to the “background” signal unless they are explicitly removed. However, this effect is small for the GWTC-3 dataset we consider: in [74], we calculate that the individually-resolved BBHs contribute to Ω_{gw} at $\sim 0.3\%$ of the GWB upper limits. They hence can be excluded, allowing the joint likelihood to be written as

$$\mathcal{L}_{\text{joint}} = \mathcal{L}_{\text{FG}}\mathcal{L}_{\text{BG}}. \quad (8)$$

Population models. To apply the stochastic siren method to GW data, the source energy spectrum in Eq. (3) and the rate density $\mathcal{R}(z)$ in Eq. (2) must be computed to obtain Ω_{gw} . We address this using parametrized models for the source redshift and component mass distributions involving 12 hyperparameters (described further in [74]). For Eq. (3), we exclusively consider BBHs since they form the majority of detected compact binaries and their population properties are better-understood than other merger types [59]. Thus, we can approximate the merger energy spectra as that of an inspiralling circular binary in the Newtonian limit with source-frame masses m_1 and m_2 (as in, e.g., [94]):

$$\frac{dE_{\text{gw}}}{df_s} = \frac{(\pi G)^{2/3}}{3f_s^{1/3}} \frac{m_1 m_2}{(m_1 + m_2)^{1/3}}. \quad (9)$$

To model $\mathcal{R}(z)$, we follow [71] and fit the redshift distribution of merging binaries with a functional form of the Madau-Dickinson star formation rate [95]. This four-parameter model possesses a smooth transition between two power-law distributions with a peak at redshift z_p and a local merger rate density $R_0 = \mathcal{R}(z=0)$. As motivated by GWTC-3 observations [96], we model the BBH mass distribution using the **PowerLaw+Peak** model [97, 98], an eight-parameter function consisting of a truncated power-law component and a Gaussian component for the primary mass and a power-law distribution

of mass ratios. Both the primary mass and mass ratio distributions are smoothly tapered at low masses.

We neglect correlations between the mass and redshift distributions. Some correlation between these parameters is expected due to metallicity variation of progenitor stars [99] and variation in the delay time of BBH formation and merger [100–102], which may influence population parameter inference [103, 104] and thus may affect resulting H_0 constraints. However, recent work suggests that such a correlation is unlikely to be relevant or required for BBH data as of GWTC-3 [105].

Beyond the 12 population parameters described above, we include three cosmological parameters. As in [39], we consider H_0 , the present-day matter energy density $\Omega_{m,0}$, and one parameter for the dark energy equation of state $w(z) = w_0$ (which enters Ω_{gw} via $E(z)$). This yields a total of 15 parameters for our full inference.

Posterior distribution construction. To measure H_0 , each likelihood must be computed given available data. For \mathcal{L}_{FG} , we must evaluate the likelihood of observed BBHs given $\vec{\lambda}$. For \mathcal{L}_{BG} , we must compute Ω_{gw} given $\vec{\lambda}$ and determine the associated likelihood of that value of Ω_{gw} .

To evaluate \mathcal{L}_{FG} , we use the ICAROGW [87] hyperparameter posteriors from the GWTC-3 population analysis [39, 59], which considered BBH mergers with signal-to-noise ratios (SNR) greater than 11. We generate a 15-dimensional kernel density estimator (KDE) using these posteriors, providing a probability function of a given $\vec{\lambda}$.

For \mathcal{L}_{BG} , we consider a power-law form of Ω_{gw} with spectral index $\alpha = 2/3$, corresponding to a compact binary GWB [78], with a reference frequency of 25 Hz as in GWTC-3 GWB searches [58, 59]. We note that \mathcal{L}_{BG} can be evaluated using the existing posteriors of Ω_{gw} obtained from previous GWB searches [58], if we prescribe a uniform prior on Ω_{gw} . According to Bayes’ theorem:

$$p_{\text{BG}}(\Omega_{\text{gw}}|\hat{C}) \propto \pi_{\text{BG}}(\Omega_{\text{gw}})\mathcal{L}_{\text{BG}}(\hat{C}|\Omega_{\text{gw}}), \quad (10)$$

where p_{BG} and π_{BG} are the posterior and prior distributions for Ω_{gw} , respectively. If we consider a uniform prior, then we can invert Eq. (10) for the likelihood:

$$\mathcal{L}_{\text{BG}}(\hat{C}|\Omega_{\text{gw}}) \propto p_{\text{BG}}(\Omega_{\text{gw}}|\hat{C}). \quad (11)$$

We obtain p_{BG} using the posterior of $\Omega_{\alpha=2/3}$ constructed from the data obtained during the first three LVK observing runs [58], under a uniform π_{BG} , allowing us to compute \mathcal{L}_{BG} . We use the $\Omega_{\alpha=2/3}$ posterior samples to generate a 1-dimensional KDE to estimate \mathcal{L}_{BG} as a function of Ω_{gw} within the range covered by the prior of $\Omega_{\alpha=2/3}$. Then, since Ω_{gw} is just a function of $\vec{\lambda}$, we can evaluate \mathcal{L}_{BG} using population and cosmological parameters.

These two individual likelihoods compose the joint likelihood of Eq. (8) as a function of 15 (hyper)parameters. We perform nested sampling [106, 107] over these parameters to compute $\mathcal{L}_{\text{joint}}$ using the **dynesty** sampler [108], as implemented in the **bilby** package [109].

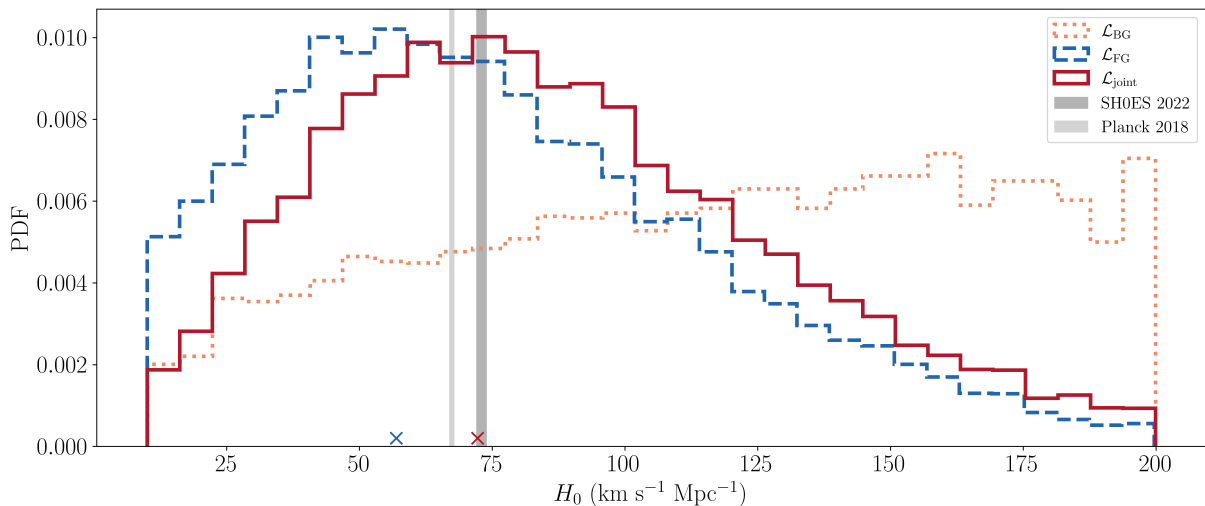


FIG. 1. Posterior distributions of the Hubble constant obtained with the spectral siren (\mathcal{L}_{FG} , dashed blue), the GWB search (\mathcal{L}_{BG} , dotted orange), and the stochastic siren joint measurement ($\mathcal{L}_{\text{joint}}$, red), each respectively marginalized over their 14 other parameters. Since no GWB has been detected, \mathcal{L}_{BG} shows less support for lower values of H_0 . Combining this with the foreground shifts the posterior, as indicated by the maximum a-posteriori probabilities for \mathcal{L}_{FG} and $\mathcal{L}_{\text{joint}}$ shown by \times markers (no marker is shown for \mathcal{L}_{BG} since the GWB non-detection provides only a lower bound on H_0). The joint measurement shifts slightly closer to the Hubble tension region vertically demarcated by the *Planck* [2] and SH0ES [6] values.

Analysis of GW observing runs. We present the results of applying the stochastic siren method to GWTC-3 data in Fig. 1. In addition to the full $\mathcal{L}_{\text{joint}}$ result (solid red), we compare with the results obtained when considering only the foreground (\mathcal{L}_{FG} , dashed blue) and background (\mathcal{L}_{BG} , dotted orange) populations. Since a uniform prior is prescribed for the population-model hyperparameters and cosmological parameters, all likelihood distributions are proportional to the corresponding posterior probability distribution, which is a function of H_0 . We show the H_0 values from *Planck* [2] and SH0ES [6] as vertical light- and dark-gray regions, respectively.

Observe that the measurement accuracy of H_0 from $\mathcal{L}_{\text{joint}}$ is improved over that from \mathcal{L}_{FG} . Specifically, the H_0 posterior obtained via $\mathcal{L}_{\text{joint}}$ peaks at a value that is closer to both the *Planck* and SH0ES values, which indicates improved consistency between GW and electromagnetic measurements of H_0 . This can be seen when comparing the maximum a-posteriori probabilities of each method: 72_{-37}^{+44} km s $^{-1}$ Mpc $^{-1}$ for $\mathcal{L}_{\text{joint}}$ versus 57_{-35}^{+43} km s $^{-1}$ Mpc $^{-1}$ for \mathcal{L}_{FG} or 46_{-26}^{+49} km s $^{-1}$ Mpc $^{-1}$ from the spectral siren [39]. Each posterior’s 68.3% highest density interval is quoted as its uncertainty. The full results for all 15 (hyper)parameters are contained in [74].

Discussion. We introduced the “stochastic siren” measurement of the Hubble constant and applied it by combining the resolved binary black hole (BBH) population with the search for the gravitational-wave background (GWB). We have shown that the GWB’s cosmological dependence allows it to aid in the measurement of H_0 , as evidenced in our analysis of the LVK’s first three observ-

ing runs. We found increased accuracy versus the spectral siren method, even though the GWB has yet to be detected. This improvement is characterized by a shift of the maximum a-posteriori probability from lower H_0 values to values more consistent with electromagnetic measurements. Note that this is a conservative result since we considered only BBHs, while the GWTC-3 GWB search results [58] are for all merger types and thus favor values of Ω_{gw} higher than what BBHs alone could produce. Lower values of Ω_{gw} are hence less probable, increasing the posterior support for higher values of H_0 .

This could be addressed in future extensions of our current stochastic siren methodology. Other mergers classes can contribute to the GWB comparably to BBHs [58, 59], which would enhance the stochastic siren method at the cost of additional population modeling and observations. We also considered only a single set of BBH population models in this work, but a variety of population models could be used. Aside from compact object mergers, other GW sources could produce observable GWBs [110, 111], which could likewise be included. Finally, as in [112], the proper integration of our method with existing population, stochastic, and cosmology analysis systems in the LVK [e.g., 40, 87, 98, 113–115] would help improve cosmological constraints as LVK observing runs continue.

As current observing runs progress, a continued non-detection of the GWB should raise the lower bound of H_0 , thereby progressively improving the precision of the measurement. This may allow the stochastic siren to serve a unique role in the Hubble tension by probing the lower early-universe measurement of H_0 in advance of the

higher late-universe measurements. Moreover, the LVK detectors are expected to observe the GWB in coming years [57, 116, 117], at which point the stochastic siren would yield even stronger improvements on the measurement of H_0 . Our current projections [74] suggest that the GWB could be detected with an SNR of eight in less than a year using the anticipated A# detector upgrades. In these projections, we also consider a variety of different cosmological and population parameters, showing what regions of parameter space will be probed by the detection or non-detection of the GWB. This highlights that the GWB is sensitive to the full expansion history of the Universe and thus depends on other cosmological parameters such as Ω_m and w_0 . While we show in [74] that the current GWB non-detection cannot constrain these parameters, the stochastic siren could in principle aid in these measurements.

The future utility of combining resolved and unresolved BBHs for population and cosmological inference should be further explored through mock data analyses. A first step in this direction is made by [112], wherein this method is applied to simulations of two years of observations during a future LVK O5 observing run, further improving H_0 measurement accuracy, albeit with a different mass model and a fixed value of w_0 . The full effect of the stochastic siren could be further explored via a mock data analysis that includes the detection of the GWB, such as during the post-O5 A# detector upgrades [118].

While upcoming LVK observing runs and upgrades are expected to enable the detection of the GWB, next-generation ground-based detectors are expected to come online soon after [119–124]. However, the GWB observed by these future detectors is expected to be non-Gaussian and non-stationary [125], which would require modifications to the current approach of GWB analysis. Moreover, the assumption of independent likelihoods used to construct the joint likelihood (Eq. (8)) may also need to be revised given the greater number of resolved mergers.

Thus, there are various avenues to extend the stochastic siren approach, but it can already inform current investigations of the Hubble tension as an entirely novel cosmological probe. It is one of the very few methods that can measure H_0 entirely independently of electromagnetic observations, allowing it to complement both GW and electromagnetic H_0 measurements. This will culminate with the eventual detection of the GWB and its resulting cosmological constraints, framing the stochastic siren as a promising tool for cosmology.

Acknowledgements. We thank the authors of [112] for constructive coordination and feedback during internal LVK review of this work. We also thank the anonymous referees for their helpful feedback. B.C. acknowledges that this material is based upon work supported by the NSF Graduate Research Fellowship Program under Grant No. DGE 21-46756. K. S. would like to acknowledge the NSF Graduate Research Fellowship Pro-

gram under Grant No. DGE-1746047 and the NSF under award PHY-2207650. A.K.W.C and N.Y. acknowledge the support from the Simons Foundation through Award No. 896696, the NSF through award PHY-2207650 and NASA through Grant No. 80NSSC22K0806. C. T. and T. C. are supported by the Eric and Wendy Schmidt AI in Science Postdoctoral Fellowship, a Schmidt Sciences program. D.E.H is supported by NSF grant PHY-2110507, and by the Kavli Institute for Cosmological Physics through an endowment from the Kavli Foundation and its founder Fred Kavli. This work made use of the Illinois Campus Cluster, a computing resource that is operated by the Illinois Campus Cluster Program (ICCP) in conjunction with the National Center for Supercomputing Applications (NCSA) and which is supported by funds from the University of Illinois at Urbana-Champaign. This material is based upon work supported by National Science Foundation (NSF) LIGO Laboratory, which is a major facility fully funded by the NSF. This work made use of `astropy` [126–128], `bilby`[109], `h5py` [129], `matplotlib` [130], `numpy` [131], and `scipy` [132]. The Supplemental Material [74] includes additional citations not referenced in the main text [133–144].

Supplemental Material for “The Stochastic Siren: Astrophysical Gravitational-Wave Background Measurements of the Hubble Constant”

COSMOLOGY AND THE GWB

Definitions

We first make cosmological definitions with the Hubble parameter $H(z)$ and present-day cosmological density parameters for radiation, matter, curvature, and dark energy ($\Omega_{r,0}$, $\Omega_{m,0}$, $\Omega_{k,0}$, and $\Omega_{DE,0}$ respectively, with dark energy’s energy density ρ_{DE}) for a generic w CDM model:

$$H(z) = H_0 \left[(1+z)^4 \Omega_{r,0} + (1+z)^3 \Omega_{m,0} + (1+z)^2 \Omega_{k,0} + \Omega_{DE,0} \frac{\rho_{DE}(z)}{\rho_{DE,0}} \right]^{1/2}, \quad (12)$$

which allows us to define $E(z)$ as:

$$E(z) \equiv \frac{H(z)}{H_0} = \left[(1+z)^4 \Omega_{r,0} + (1+z)^3 \Omega_{m,0} + (1+z)^2 \Omega_{k,0} + \Omega_{DE,0} \frac{\rho_{DE}(z)}{\rho_{DE,0}} \right]^{1/2}. \quad (13)$$

In our analysis, we consider only a flat universe with negligible radiation, so $\Omega_{k,0} = \Omega_{r,0} = 0$, then $\Omega_{DE,0} = 1 - \Omega_{m,0}$. Eq. (13) then becomes

$$E(z) \equiv \frac{H(z)}{H_0} = \left[(1+z)^3 \Omega_{m,0} + (1 - \Omega_{m,0}) \frac{\rho_{DE}(z)}{\rho_{DE,0}} \right]^{1/2}. \quad (14)$$

We next define the requisite distance measures:

- Hubble distance:

$$D_H \equiv c/H_0 \quad (15)$$

- line-of-sight comoving distance:

$$D_C = \frac{c}{H_0} \int_0^z \frac{dz}{E(z)} = D_H \int_0^z \frac{dz}{E(z)} \quad (16)$$

- transverse comoving distance:

$$D_M = \begin{cases} D_H \frac{1}{\sqrt{\Omega_k}} \sinh [\sqrt{\Omega_k} D_C/D_H] & \text{for } \Omega_k > 0 \\ D_C & \text{for } \Omega_k = 0 \\ D_H \frac{1}{\sqrt{|\Omega_k|}} \sin [\sqrt{|\Omega_k|} D_C/D_H] & \text{for } \Omega_k < 0 \end{cases} \quad (17)$$

- angular diameter distance:

$$D_A = \frac{D_M}{1+z} = \frac{D_C}{1+z} \text{ when } \Omega_k = 0 \quad (18)$$

- luminosity distance:

$$D_L = (1+z)D_M = (1+z)D_C \text{ when } \Omega_k = 0 \quad (19)$$

E(z) for parametrized dark energy

Using the dark energy equation-of-state parameter $w(z)$, we follow [136] and write the dark energy evolution term in Eq. (14) as

$$\frac{\rho_{DE}(z)}{\rho_{DE,0}} = \exp \left[3 \int_0^{\ln(1+z)} d \ln(1+z') [1 + w(z')] \right]. \quad (20)$$

We next modify this term using a parametrization of $w(z)$. In general, $w(z)$ can be solved for under a specific scalar field theory, or is more generically parametrized. In this work, however, we assume a constant equation of state parameter ($w(z) = w_0$, as in [39]). Then, the integral in the exponential can be solved analytically: let $y \equiv \ln(1+z)$, so the integral becomes

$$\left[\int_0^y dy (1 + w_0) \right] = y(1 + w_0) = \ln(1+z)(1 + w_0), \quad (21)$$

which allows the exponential to be rewritten as

$$\exp[3 \ln(1+z)(1 + w_0)] = (1+z)^{3(1+w_0)}. \quad (22)$$

Equation (14) is then simply

$$E(z, w_0, \Omega_{m,0}) = \left[(1+z)^3 \Omega_{m,0} + (1 - \Omega_{m,0})(1+z)^{3(1+w_0)} \right]^{1/2}. \quad (23)$$

Derivation of the GWB energy density

We derive Ω_{gw} as arising from astrophysical mergers, generally following the procedure of earlier work [61, 76–78, 142] while avoiding the occasional error of incorrect cosmological distances and/or frames that can result in incorrect factors of $(1+z)$ as noted in [137]. Note that for consistency with current LVK convention, we express frequencies as f instead of the occasionally-used ν ; we hence express the fluence here as \mathcal{F} instead of f .

The dimensionless energy density Ω_{gw} for an astrophysical GWB is typically expressed as:

$$\Omega_{\text{gw}} = \frac{f}{\rho_c c^3} F(\vec{\phi}, f) \quad (24)$$

where $f = f_s/(1+z)$ is the observer-frame GW frequency in terms of the source-frame frequency f_s and F is the integrated flux of the astrophysical sources:

$$F(\vec{\phi}, f) = \int p(\vec{\phi}) \int \mathcal{F}(\vec{\phi}, f) \frac{d\dot{N}^\circ(\vec{\phi}, z)}{dz} d\vec{\phi} dz, \quad (25)$$

for source parameters $\vec{\phi}$ and associated probability distribution $p(\vec{\phi})$, source fluence $\mathcal{F}(\vec{\phi}, f)$ (flux times time), and the total number of events per unit observer time per redshift interval $d\dot{N}^\circ(\vec{\phi}, z)/dz$.

We first consider the fluence, which is the energy per unit area A per unit frequency. We take its definition (in source frame and frequency) as Eq. (2.45) of [141]:

$$\mathcal{F}(\vec{\phi}, f) \equiv \frac{dE}{dA df} = \frac{(1+z)^2}{D_L^2} \frac{dE_{\text{gw}}(\vec{\phi}, f_s)}{d\Omega df_s} = \frac{(1+z)^2}{(1+z)^2 D_C^2} \frac{dE_{\text{gw}}(\vec{\phi}, f_s)}{d\Omega df_s} = \frac{1}{D_C^2} \frac{dE_{\text{gw}}(\vec{\phi}, f_s)}{d\Omega df_s} \quad (26)$$

where we have used the luminosity distance as defined in Eq. (19) and introduced the solid angle differential $d\Omega$. Note here that the emitted gravitational spectral energy is $dE_{\text{gw}}(\vec{\phi}, f)/df_s$, as used in Eq. (3) of the main text.

We next consider the total number of events per unit *observer* time, per redshift interval,

$$\frac{d\dot{N}^\circ(\vec{\phi}, z)}{dz} = \mathcal{R}^\circ(\vec{\phi}, z) \frac{dV}{dz}(z), \quad (27)$$

for observer-frame comoving event rate density \mathcal{R}° and comoving volume element

$$dV_C = D_H \frac{(1+z)^2 D_A^2}{E(z)} d\Omega dz = \frac{c}{H_0} \frac{D_C^2}{E(z)} d\Omega dz. \quad (28)$$

Combining Equations (27) and (28) yields

$$\frac{d\dot{N}^\circ(\vec{\phi}, z)}{dz} = \mathcal{R}^\circ(\vec{\phi}, z) \frac{c}{H_0} \frac{D_C^2}{E(z)} d\Omega. \quad (29)$$

To match current literature, we next convert to *source* time. This requires redshifting to the source-frame comoving rate density $\mathcal{R} = (1+z)\mathcal{R}^\circ$ (since time redshifts as $t_s = t/(1+z)$), so we rewrite Eq. (29) as

$$\frac{d\dot{N}^\circ(\vec{\phi}, z)}{dz} = \frac{\mathcal{R}(\vec{\phi}, z)}{(1+z)} \frac{c}{H_0} \frac{D_C^2}{E(z)} d\Omega. \quad (30)$$

We then assemble the integrated flux by inserting Eq. (26) and Eq. (30) into Eq. (25):

$$\begin{aligned} F(\vec{\phi}, f) &= \int p(\vec{\phi}) d\vec{\phi} \int \frac{1}{D_C^2} \frac{dE_{\text{gw}}(\vec{\phi}, f_s)}{d\Omega df_s} \frac{\mathcal{R}(\vec{\phi}, z)}{(1+z)} \frac{c}{H_0} \frac{D_C^2}{E(z)} d\Omega \\ &= \frac{c}{H_0} \int \frac{\mathcal{R}(z)}{(1+z)E(z)} \int p(\vec{\phi}) \frac{dE_{\text{gw}}(\vec{\phi}, f_s)}{df_s} d\vec{\phi} dz \\ &= \frac{c}{H_0} \int \frac{\mathcal{R}(z)}{(1+z)E(z)} \left\langle \frac{dE_{\text{gw}}}{df_s} \right\rangle_{f_s} dz, \end{aligned} \quad (31)$$

where we obtain the second line by assuming no correlation between source parameters and redshift ($\mathcal{R}(z, \vec{\phi}) = \mathcal{R}(z)$) as elaborated in the main text. We obtain the third line by defining

$$\left\langle \frac{dE_{\text{gw}}}{df_s} \right\rangle_{f_s} \equiv \int p(\vec{\phi}) \frac{dE_{\text{gw}}(\vec{\phi}, f_s)}{df_s} d\vec{\phi}. \quad (32)$$

Finally, by inserting Eq. (31) into Eq. (24), we find that the GW energy density is

$$\boxed{\Omega_{\text{gw}} = \frac{f}{\rho_c c^2 H_0} \int \frac{\mathcal{R}(z)}{(1+z)E(z)} \left\langle \frac{dE_{\text{gw}}}{df_s} \right\rangle_{f_s} dz}, \quad (33)$$

which yields Eq. (2) in the main text when using the definition of the critical mass density ρ_c .

PARAMETER INFERENCE METHODS AND RESULTS

Contribution of resolved mergers to Ω_{gw}

In order for an analysis using a joint likelihood factorized into \mathcal{L}_{BG} and \mathcal{L}_{FG} to be valid, the magnitude of the resolved foreground's contributions to Ω_{gw} must be negligible relative to the total Ω_{gw} . To quantify this contribution, we discretely computed the Ω_{gw} contribution of the 42 resolved BBHs considered in our work following the formalism outlined in [133, 134]. Specifically, we write the integrated flux in Eq. (24) as

$$F(f) = T_{\text{obs}}^{-1} \frac{\pi c^3}{2G} f^2 \sum_{k=1}^N (|\tilde{h}_{+,k}|^2 + |\tilde{h}_{\times,k}|^2) \quad (34)$$

where T_{obs} is the observing time and $\tilde{h}_{+,k}^2$, $\tilde{h}_{\times,k}^2$ are respectively the Fourier transforms of the plus and cross strain polarizations for the k^{th} merger, out of N total mergers. In the circular Newtonian regime (containing the GW frequency of interest, 25 Hz), the Fourier-transformed strain polarizations are

$$|\tilde{h}_+(f)| = h_z \frac{(1 + \cos^2 \iota)}{2} f^{-7/6} \quad (35)$$

$$|\tilde{h}_\times(f)| = h_z \cos \iota f^{-7/6}. \quad (36)$$

Here, the amplitude of the signal is

$$h_z = \sqrt{\frac{5}{24}} \frac{[GM(1+z)]^{5/6}}{\pi^{2/3} c^{3/2} D_L(z)}, \quad (37)$$

for source-frame chirp mass \mathcal{M} .

Inserting Eq. (34)-(37) into Eq. (24) yields

$$\Omega_{\text{gw}}(f, \mathcal{M}, z, \iota) = \frac{5\pi^{2/3} G^{5/3}}{18c^3 H_0^2} f^{2/3} \sum_{k=1}^N \left\{ \frac{[\mathcal{M}_k(1+z_k)]^{5/3}}{D_L(z_k)^2} \left[\frac{(1+\cos^2 \iota_k)^2}{4} + \cos^2 \iota_k \right] \right\}. \quad (38)$$

In this form, Ω_{gw} can be computed a function of the source parameters for each individual merger. Using the posterior medians from the GWTC-3 catalog [73] for the chirp masses, redshifts, and inclinations of the 42 BBHs involved in our work (with $T_{\text{obs}} = 2$ years given ~ 4 months of O1, ~ 9 months of O2, and ~ 11 months of O3), we found that their contribution is $\sim 2.3 \times 10^{-11}$ at 25 Hz. Compared with the most recent estimate for the total $\Omega_{\text{gw}} \sim 6.9 \times 10^{-10}$ at 25 Hz [59], the resolved mergers contribute $\sim 3.3\%$ to the expected total energy density. This means that the resolved mergers' contribution is $\sim 0.2\%$ of the GWTC-3 upper limit result [58] that we considered in our analysis ($\sim 1.2 \times 10^{-8}$) and hence is largely negligible for the purposes of our inference.

Furthermore, the upper limit is a factor of $\sim 17\times$ higher than the expected total Ω_{gw} [59] ($\sim 1.2 \times 10^{-8}$ versus $\sim 6.9 \times 10^{-10}$). This implies that the upper limit data will result in conservative (higher) measurements of H_0 . This is because the unresolved contribution to Ω_{gw} will always be lower than the total (resolved plus unresolved), and hence the upper limits (which are on the total Ω_{gw} , not just the unresolved component) will favor values of Ω_{gw} higher than what these unresolved mergers could produce alone. Given this, there is more posterior support for lower values of H_0 (i.e., a worse measurement, in the same way that considering only BBHs leads to conservative results when compared to including BNSs and NSBHs).

Population models

We describe the mass and redshift population models used in our inference, which we selected in order to compare with previous results [39]. For a description of the **PowerLaw+Peak** mass model, we refer to existing sources [96–98] and its implementation via equations B.10-12 in [87]. For the redshift model, we use a functional form of the Madau-Dickinson model [95] as parametrized in [71]:

$$\mathcal{R}(z) = [1 + (1 + z_p)^{-\gamma-\kappa}] \frac{(1+z)^\gamma}{1 + \left(\frac{1+z}{1+z_p}\right)^{\gamma+\kappa}} R_0. \quad (39)$$

As noted in [71], this parametrization subsumes some astrophysical effects on the BBH population, such as formation-to-merger time delays, without needing to explicitly model them.

Table I contains descriptions of these population hyperparameters, as well as the uniform priors used for all population and cosmological parameters in the inference.

Analysis validation

For all results of \mathcal{L}_{FG} , \mathcal{L}_{BG} , and $\mathcal{L}_{\text{joint}}$, we ensured convergence by checking consistency between results obtained using lower (2048) and higher (3072) counts of live points, as is conventional in nested sampling analysis.

The kernel density estimators (KDEs) used in our analysis were each a standard gaussian-kernel KDE. These were generated with SciPy and its default settings in `scipy.stats.gaussian_kde` [145], which automatically select the bandwidth scale based on the dataset according to one of two default bandwidth selection methods. To check for consistency, we used each of these two KDE bandwidth selection methods (the ‘‘Scott’s Rule’’ and Silverman methods) for the analysis and found no appreciable differences in the results.

Generating the KDE for \mathcal{L}_{BG} required boundary effect remediation, given that the Ω_{gw} upper limit posterior from [58] peaks at ~ 0 , which would cause a naive KDE approach to create an anomalously-vanishing probability as $\Omega_{\text{gw}} \rightarrow 0$. We remedied this by mirroring the underlying posterior distribution and generating the KDE from that while accounting for renormalization, as has been performed previously (e.g., described in Appendix B of [135]). This

Parameter	Description	Prior
<i>Mass model parameters</i>		
α	Index of power law primary mass	$\mathcal{U}(1.5, 12)$
β	Index of power law secondary mass	$\mathcal{U}(-4, 12)$
m_{min}	Minimum mass	$\mathcal{U}(2M_{\odot}, 10M_{\odot})$
m_{max}	Maximum mass	$\mathcal{U}(50M_{\odot}, 200M_{\odot})$
λ_g	Fraction of events in Gaussian	$\mathcal{U}(0, 1)$
μ_g	Peak of Gaussian	$\mathcal{U}(20M_{\odot}, 50M_{\odot})$
σ_g	Width of Gaussian	$\mathcal{U}(0.4M_{\odot}, 10M_{\odot})$
δ_m	Range of tapering function	$\mathcal{U}(0M_{\odot}, 10M_{\odot})$
<i>Population hyperparameters</i>		
R_0	The BBH merger rate at $z = 0$	$\mathcal{U}(0, 100)$
γ	Index for the power law before z_p	$\mathcal{U}(0, 12)$
κ	Index for the power law after z_p	$\mathcal{U}(0, 6)$
z_p	Peak redshift	$\mathcal{U}(0, 4)$
<i>Cosmological parameters</i>		
$\Omega_{m,0}$	Present matter energy density	$\mathcal{U}(0, 1)$
w_0	Dark energy equation of state parameter	$\mathcal{U}(-3, 0)$
H_0	Hubble constant	$\mathcal{U}(10, 200)$

TABLE I. A summary of the parameters considered and the uniform priors \mathcal{U} used for parameter inference. The population models involve the eight-parameter **PowerLaw+Peak** mass model [96–98] and the four-parameter Madau-Dickinson redshift distribution [95], yielding a total of 15 parameters when combined with three cosmological parameters.

boundary effect was not present for the 15 hyperparameter posteriors from [39], as mirroring either did not affect the results, or distorted the KDE and thus made it *less* representative of the posterior distribution.

Finally, if our KDE method is to be consistent with the full hierarchical likelihood evaluation utilized by standard population analysis methods, the BBH spectral siren results of [39] should be recovered given that we adopted their population hyperparameter posteriors to construct the \mathcal{L}_{FG} KDE. We found that the results of \mathcal{L}_{FG} are directly comparable to the H_0 results obtained via the BBH spectral siren method of [39], whose maximum a-posteriori probability and 68.3% highest density interval is reported as 46_{-26}^{+49} km s⁻¹ Mpc⁻¹. We recover a result consistent with theirs: 57_{-35}^{+43} km s⁻¹ Mpc⁻¹. We similarly obtain consistent results for the 14 other hyperparameters in [39], indicating that the posterior-generated KDE is a reasonable proxy for a full hierarchical population analysis approach.

Other parameter results

We show our inference results for the redshift model and cosmological parameters in Fig. 2. Note that in general, measurements of most hyperparameters are not greatly altered by the inclusion of the GWB non-detection.

However, observe that the redshift model hyperparameter γ (the exponent governing the lower-redshift merger rate, as in Eq. (39)) has some marginal improvement, namely a tendency toward lower value. This is sensible given that the upper limit on Ω_{gw} will favor lower values of γ since larger γ implies more mergers, and thus a larger Ω_{gw} . There is hence some correlation between H_0 and these parameters; the findings of [112] are consistent with this result. We also note that while the \mathcal{L}_{joint} posteriors for $\Omega_{m,0}$ and z_p are shifted slightly relative to \mathcal{L}_{FG} , the posteriors themselves are too broad to offer informative constraints.

Our parameter inference also considered eight mass model hyperparameters, but the posteriors are effectively unchanged by the inclusion of the GWB (see Fig. 3), indicating no improvement in constraining these parameters.

SNR OF THE GWB AND PROJECTIONS FOR FUTURE DETECTORS

The optimal SNR of the GW energy density Ω_{gw} in a given detector network is given by [75]

$$\langle \text{SNR} \rangle_{\text{opt}} = \sqrt{(\gamma \Omega_{gw} | \gamma \Omega_{gw})}, \quad (40)$$

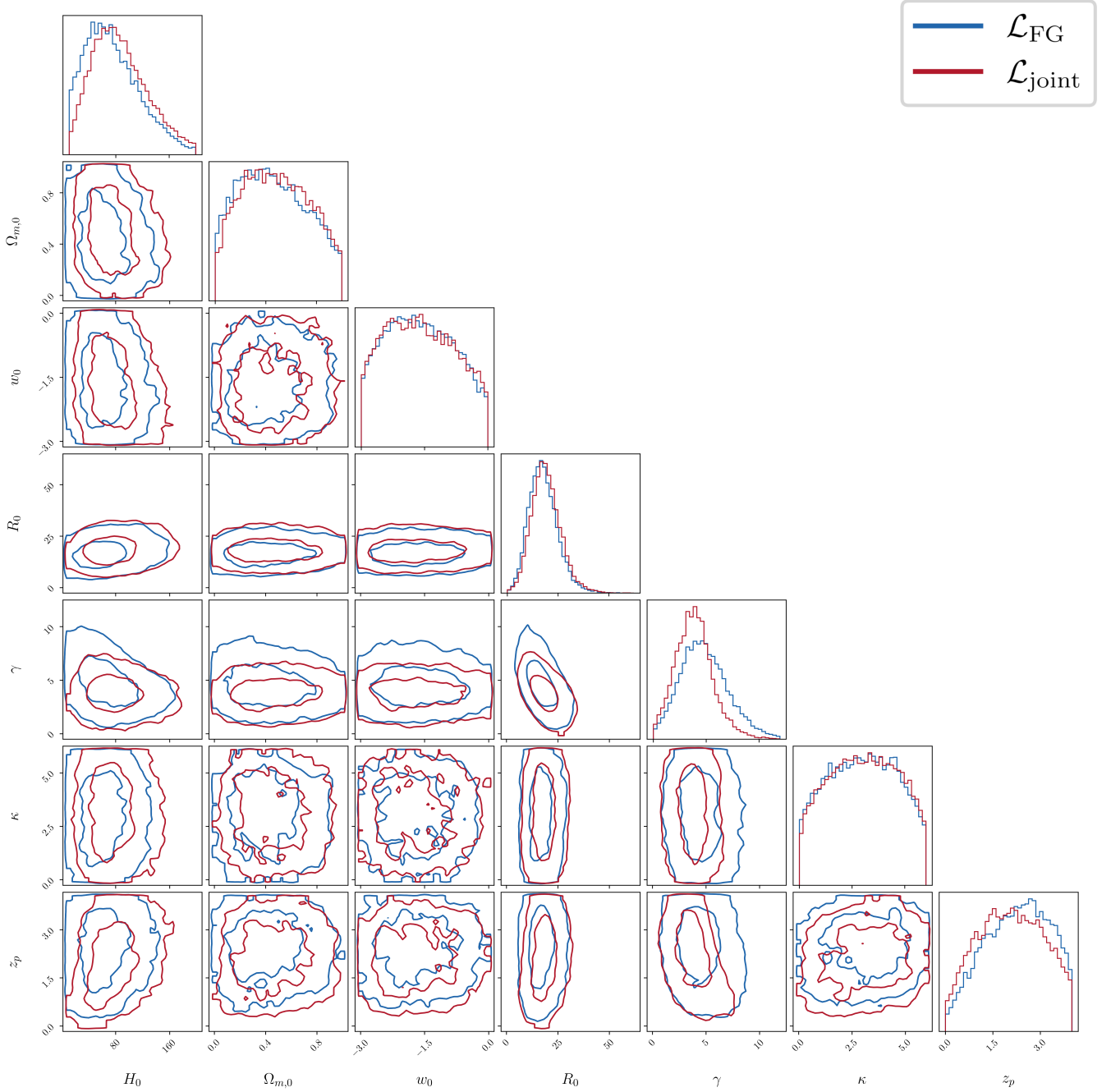


FIG. 2. Redshift model hyperparameters, together with cosmological parameters, as inferred via the BBH spectral siren (\mathcal{L}_{FG} , blue) and stochastic siren ($\mathcal{L}_{\text{joint}}$, red) methods. Observe that most hyperparameters do not demonstrate an improvement with the current non-detection of the BBH GWB, with the exception of γ as elaborated in the text.

where γ is the overlap reduction function and the inner product is defined in the main text. We can then write the SNR as

$$\langle \text{SNR} \rangle_{\text{opt}} = \sqrt{2T \left(\frac{3H_0^2}{10\pi^2} \right)^2 \int_0^\infty df \frac{\gamma^2 \Omega_{\text{gw}}^2}{f^6 P_1(f) P_2(f)}}, \quad (41)$$

noting how it scales with the Hubble constant ($\Omega_{\text{gw}} \sim H_0^{-3} \Rightarrow \text{SNR} \sim H_0^{-1}$) and with observing time ($\text{SNR} \sim \sqrt{T}$). From this scaling, it is clear that a longer observing time increases the chance of GWB detection, and that H_0 impacts

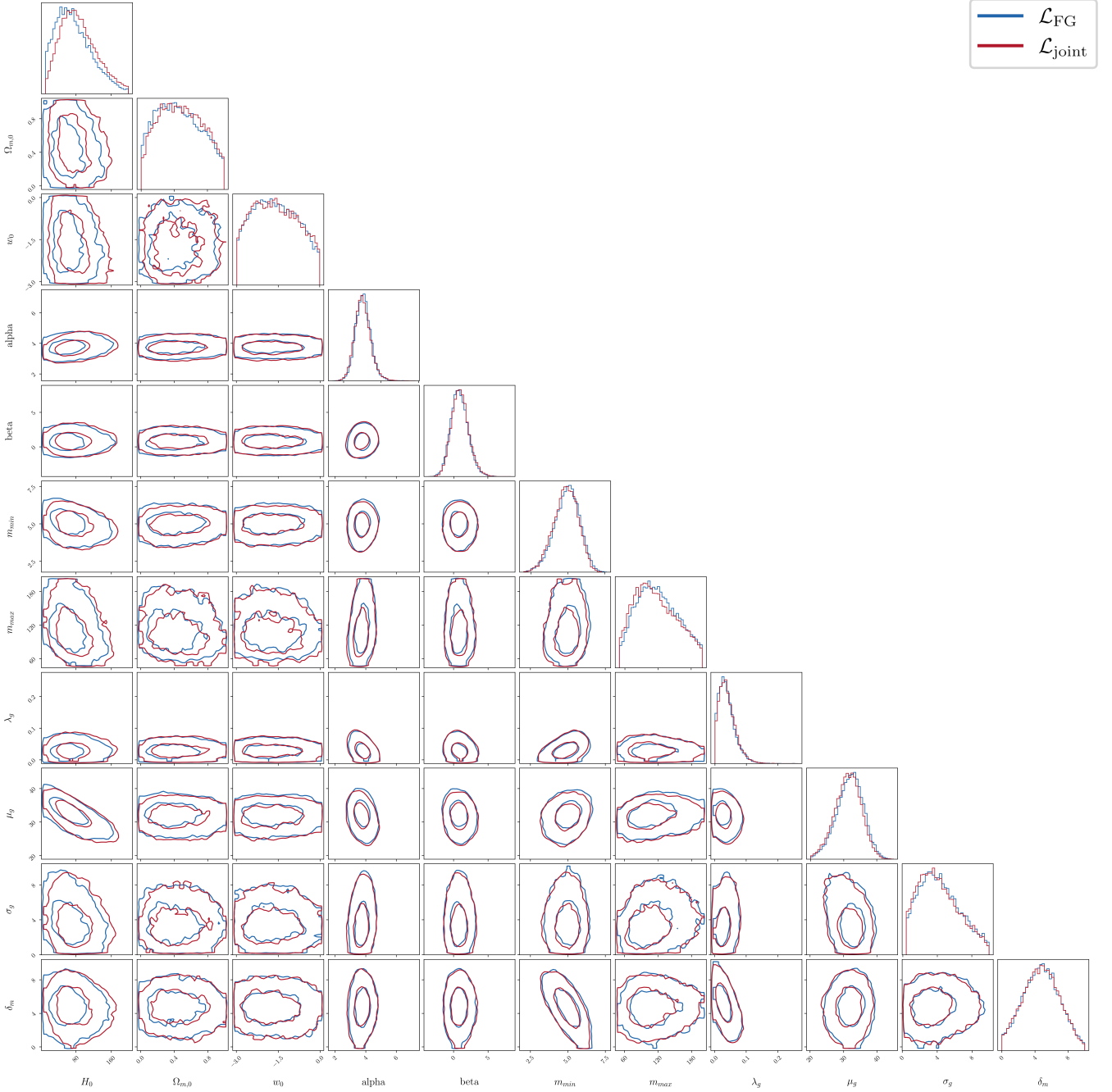


FIG. 3. Mass model hyperparameters, together with cosmological parameters, as inferred via the BBH spectral siren (\mathcal{L}_{FG} , blue) and stochastic siren ($\mathcal{L}_{\text{joint}}$, red) methods. Observe that effectively no mass hyperparameter constraints demonstrate an improvement with the current non-detection of the BBH GWB.

the time to detection that a non-detection implies larger values of H_0).

To demonstrate this scaling behavior, we make projections of the time required for GWB detection using future detector networks (Fig. 4). Note that as in the rest of this work, we are considering only the BBH contribution to Ω_{gw} . This means that our energy spectrum may be an underestimate, implying that our time-to-detection projections are conservative. Here, we pin the mass and redshift hyperparameters to their mean posterior values obtained from [39], which are $\alpha = 3.4$, $\beta = 1.08$, $m_{\text{min}} = 5.08$, $m_{\text{max}} = 86.85$, $\lambda_g = 0.04$, $\mu_g = 33.73$, $\sigma_g = 3.56$, and $\delta_m = 4.83$ for the mass model, and $R_0 = 17.975$, $\gamma = 2.7$, $\kappa = 2.9$, and $z_p = 1.9$ for the redshift distribution. For cosmological parameters, we used $\Omega_{m,0} = 0.3065$, $w_0 = -1$, $H_0 = \{67.4, 73\}$ from [2, 6]. Note that the value of $\Omega_{m,0}$ is taken from

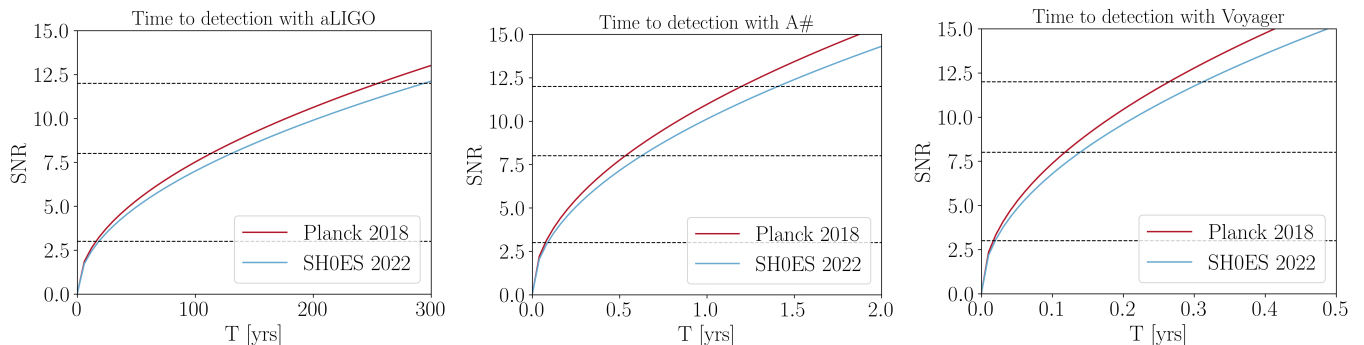


FIG. 4. The time to detect a GWB with a detector network consisting of LIGO-Hanford, LIGO-Livingston, and Virgo with the sensitivity of aLIGO, A#, or Voyager. In all plots, the dashed lines represent SNR values of three, eight, and twelve respectively, and results are shown for both the Planck [2] and SH0ES [6] values of H_0 to give an example for how time to detection changes with H_0 . Note that the time to detection is very different across these different networks, so these plots have a different scaling on the x-axis.

the Planck 2015 [144] instead of Planck 2018 in order to match LVK work [39].

We consider three different cases with the sensitivities predicted for advanced LIGO (aLIGO), A# [118], and Voyager [143]. In all cases, we conservatively assume a three-detector network composed of LIGO-Hanford, LIGO-Livingston, and Virgo, all with the same sensitivity. Adding the SNR between each pair of detectors in quadrature, we obtain the network SNR:

$$\langle \text{SNR} \rangle_{\text{net}} = \sqrt{\text{SNR}_{\text{HL}}^2 + \text{SNR}_{\text{HV}}^2 + \text{SNR}_{\text{LV}}^2}. \quad (42)$$

With these estimates, we find the time to detection in aLIGO too long to be practical (on the order of centuries of observation needed for an SNR of eight). However, A# and Voyager are more promising, with both networks capable of detecting the GWB with the assumed properties within one year. The factor of ~ 10 improvement in sensitivity between aLIGO and A# is responsible for this dramatic improvement in time to detection.

The estimates in Fig. 4 were performed assuming specific values for each of the parameters, yet it is informative to consider how the SNR can change with different combinations of the parameters. We hence show the relation between two parameters at a time (with all other parameters held fixed) in Fig. 5, with SNR as a function of the cosmological parameters $\{H_0, \Omega_{m,0}, w_0\}$ represented via either a heatmap or contour lines (for SNR values of 8 and 20). These plots illustrate which regions of parameter space could be ruled out by a non-detection of the GWB, as any combination of parameters that corresponds to an SNR larger than eight (beyond the contour line) would be measurable.

The top (middle) two plots show A# detectors after one year (two years) of observation to demonstrate the increase in SNR over time. An animation illustrating this change in SNR over time is available in the supplemental archive file. The horizontal and vertical lines respectively correspond to the best-fit parameter values and the H_0 tension values [2, 6]. The bottom two plots of Fig. 5 analogously show the SNR of the GWB, but for various networks of detectors observing for a two-year period. Figure 5 is consistent with Fig. 4, demonstrating that after two years of observation, aLIGO would not confidently detect a GWB with these parameters, while A# and Voyager would measure it with $\text{SNR} \gtrsim 20$. For completeness, additional versions of Fig. 5 that show SNR as a function of other parameters can be found below (Figs. 6 – 11).

* Corresponding author: brycec2@illinois.edu

- [1] Riess, Adam G *et al.*, *The Astronomical Journal* **116**, 1009 (1998).
- [2] Aghanim, Nabila *et al.*, *Astronomy & Astrophysics* **641**, A6 (2020).
- [3] M. Kamionkowski and A. G. Riess, *The Hubble Tension and Early Dark Energy* (2022), [arxiv:2211.04492](https://arxiv.org/abs/2211.04492) [[astro-ph](#), [physics:gr-qc](#), [physics:hep-ph](#)].
- [4] E. Di Valentino, O. Mena, S. Pan, L. Visinelli, W. Yang, A. Melchiorri, D. F. Mota, A. G. Riess, and J. Silk, *Classical and Quantum Gravity* **38**, 153001 (2021).
- [5] A. G. Riess, S. Casertano, W. Yuan, L. M. Macri, and D. Scolnic, *The Astrophysical Journal* **876**, 85 (2019).
- [6] Riess, Adam G. *et al.*, *Astrophys. J. Lett.* **934**, L7 (2022), [arXiv:2112.04510](https://arxiv.org/abs/2112.04510) [[astro-ph.CO](#)].
- [7] Brout, Dillon *et al.*, *The Astrophysical Journal* **938**, 110 (2022).

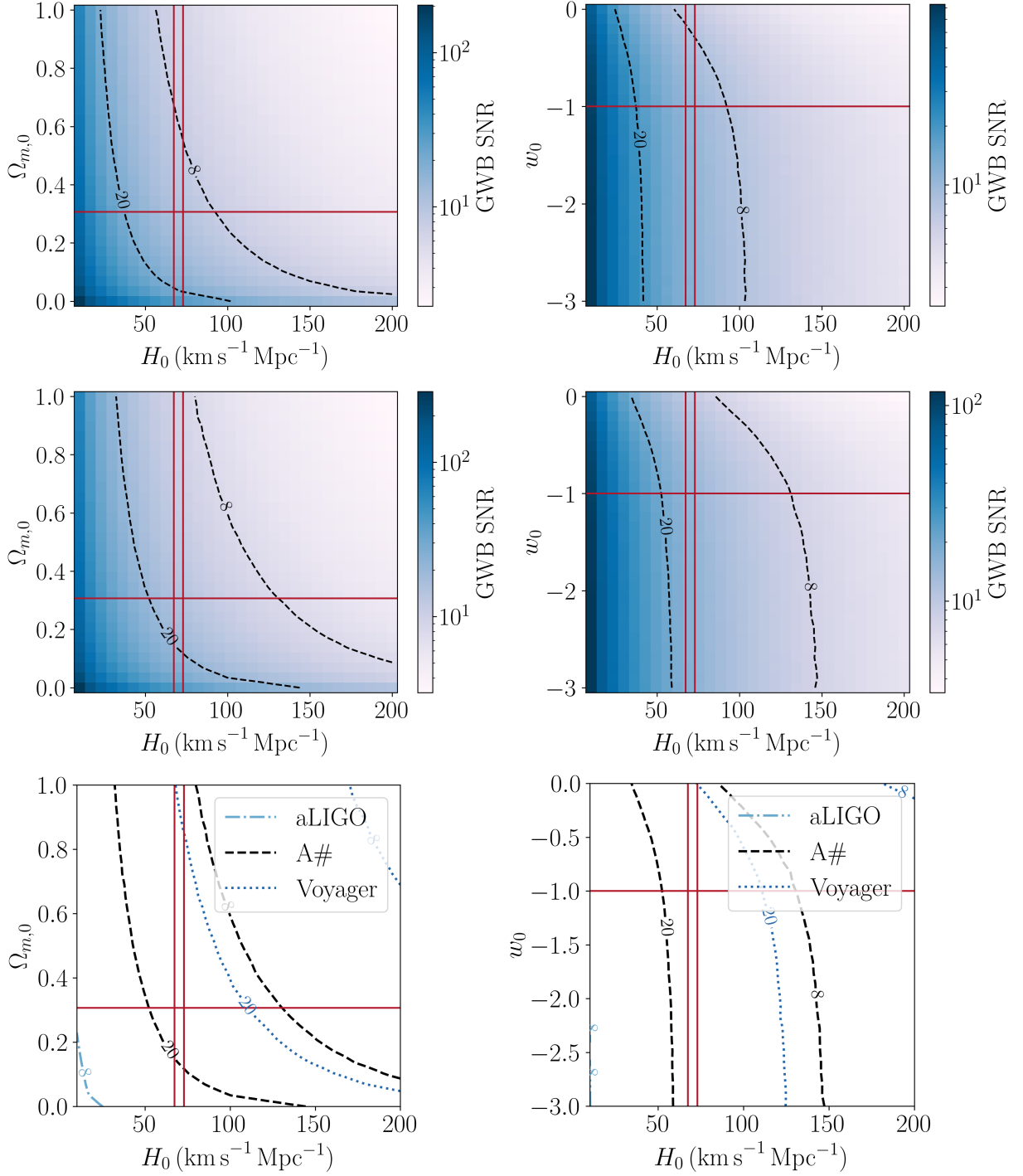


FIG. 5. SNR of the GWB for various future detector networks as a function of two cosmological parameters (H_0 with either $\Omega_{m,0}$ or w_0), with the other 13 (hyper)parameters fixed to values denoted in the text. Top (middle) plots: a network of three A# detectors after one year (two years) of observation, with SNR shown as a heatmap. Contour lines illustrate constant values of SNR = 8 and SNR = 20, while the red horizontal and vertical lines indicate existing cosmological parameter measurements. Observe that regions of parameter space that are detectable (areas with higher SNR) expand with increasing observing time, such that the GWB would be detectable within 1-2 years. Bottom: the same as the previous plots, but for networks with aLIGO, A#, and Voyager sensitivities after two years of observation. Observe that there are effectively no values of these parameters that would make the GWB measurable in aLIGO after only two years. Analogous plots that pair H_0 with population hyperparameters are shown in the remainder of this text.

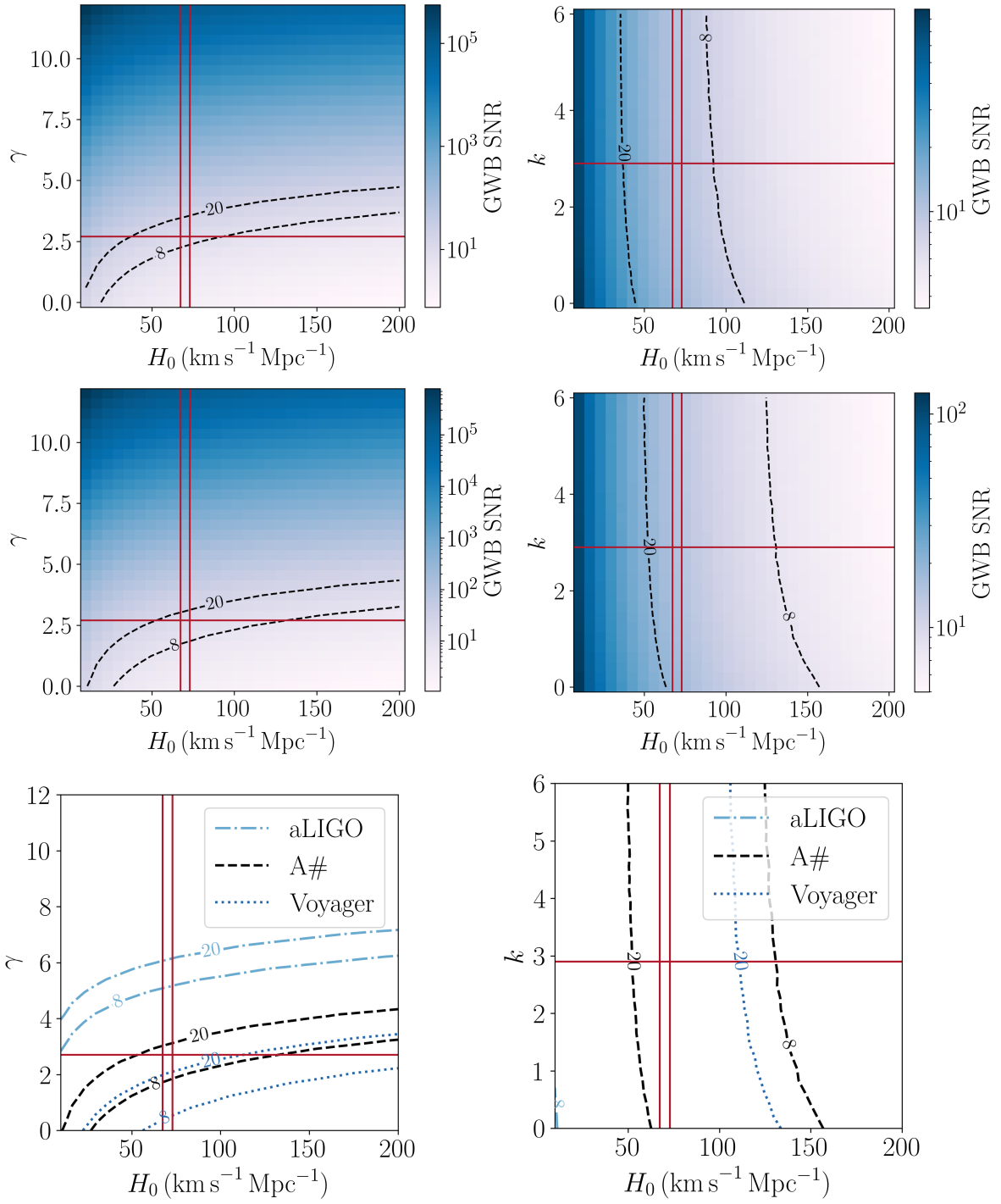


FIG. 6. SNR of the GWB for various future detector networks as a function of two parameters (H_0 with either γ or k), with the other 13 (hyper)parameters fixed to values denoted in the text. Refer to Fig. 5 for more explanation of the subplots.

- [8] W. L. Freedman, *The Astrophysical Journal* **919**, 16 (2021).
- [9] S. Suyu, P. Marshall, M. Auger, S. Hilbert, R. Blandford, L. Koopmans, C. Fassnacht, and T. Treu, *The Astrophysical Journal* **711**, 201 (2010).
- [10] Wong, Kenneth C *et al.*, *Monthly Notices of the Royal Astronomical Society* **498**, 1420 (2020).
- [11] R. Jimenez, A. Cimatti, L. Verde, M. Moresco, and B. Wandelt, *Journal of Cosmology and Astroparticle Physics* **2019** (03), 043, [arXiv:1902.07081 \[astro-ph\]](https://arxiv.org/abs/1902.07081).
- [12] Balkenhol, L. *et al.*, *Physical Review D* **108**, 023510 (2023), [arXiv:2212.05642 \[astro-ph\]](https://arxiv.org/abs/2212.05642).

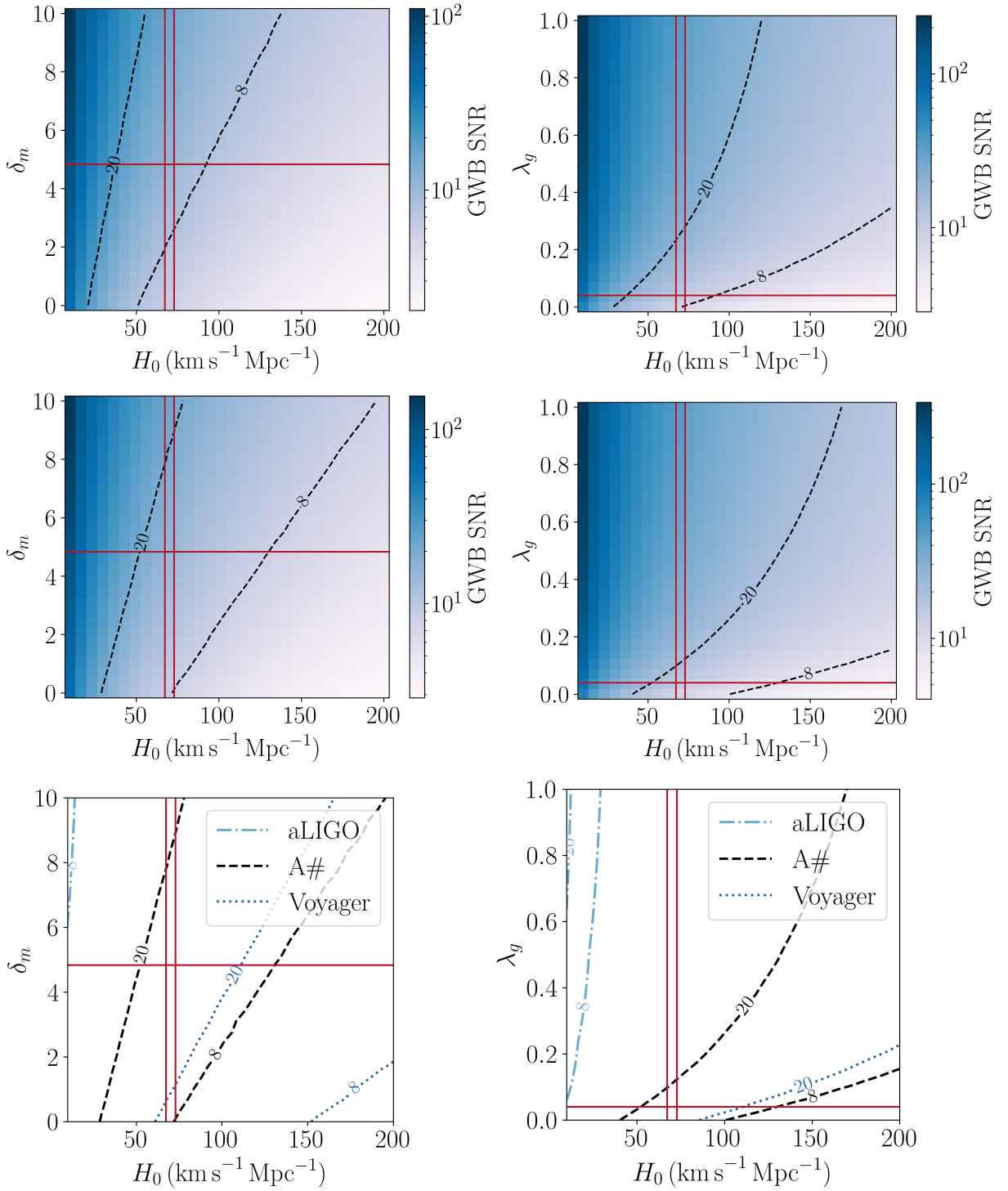


FIG. 7. SNR of the GWB for various future detector networks as a function of two parameters (H_0 with either δ_m or λ_g), with the other 13 (hyper)parameters fixed to values denoted in the text. Refer to Fig. 5 for more explanation of the subplots.

- [13] Alam, Shadab *et al.*, *Physical Review D* **103**, 083533 (2021).
- [14] Adame, A. G. and others (The DESI Collaboration) (DESI), *DESI 2024 VI: Cosmological Constraints from the Measurements of Baryon Acoustic Oscillations* (2024), arXiv:2404.03002 [astro-ph].
- [15] Macaulay, E. and others (The DES Collaboration), *Monthly Notices of the Royal Astronomical Society* **486**, 2184 (2019).
- [16] Aasi, Junaid *et al.*, *Classical and quantum gravity* **32**, 074001 (2015).
- [17] Acernese, Fausto *et al.*, *Classical and Quantum Gravity* **32**, 024001 (2014).

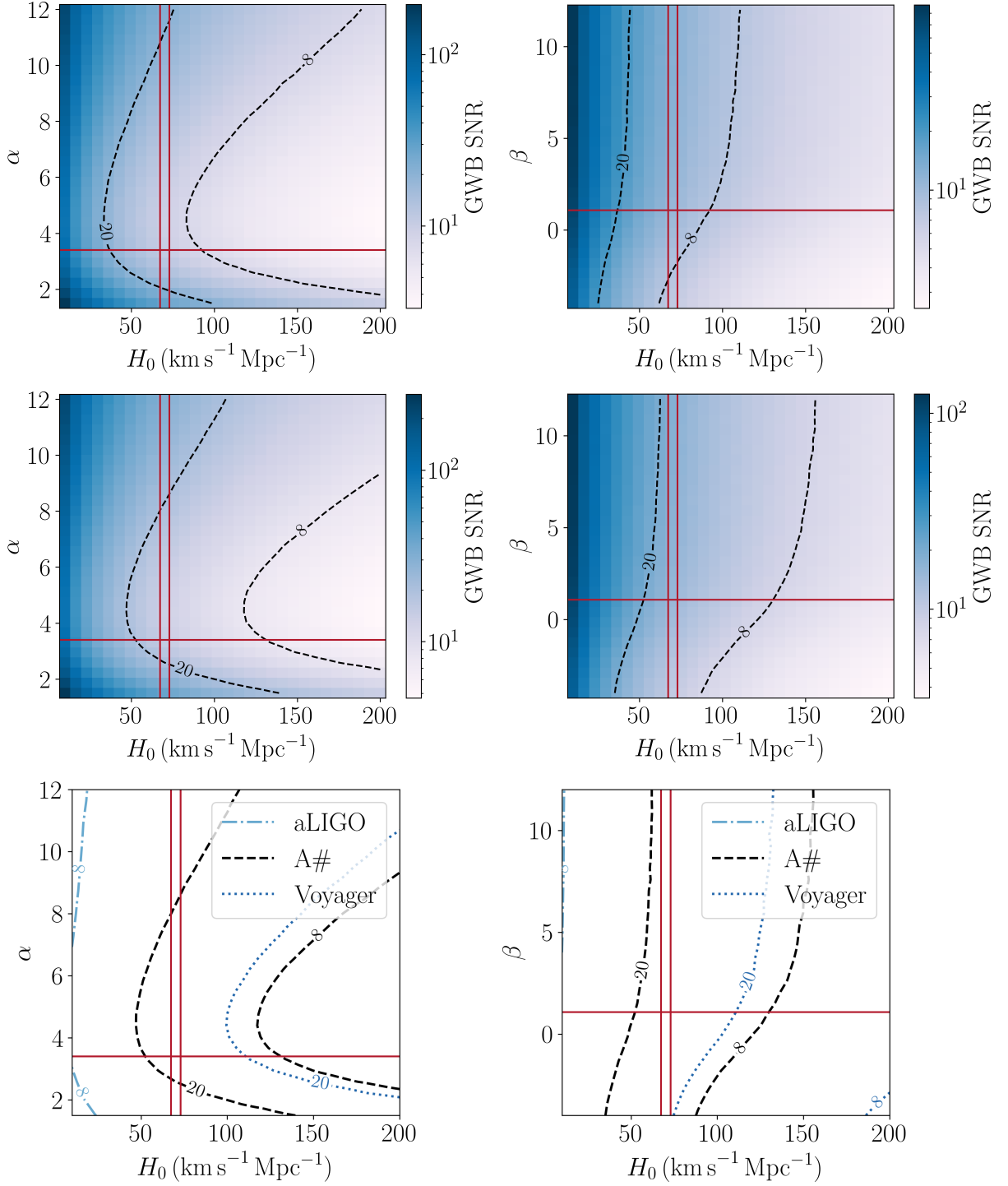


FIG. 8. SNR of the GWB for various future detector networks as a function of two parameters (H_0 with either α or β), with the other 13 (hyper)parameters fixed to values denoted in the text. Refer to Fig. 5 for more explanation of the subplots.

- [18] K. Somiya and K. Collaboration, *Classical and Quantum Gravity* **29**, 124007 (2012).
- [19] B. F. Schutz, *Nature* **323**, 310 (1986).
- [20] D. E. Holz and S. A. Hughes, *The Astrophysical Journal* **629**, 15 (2005).
- [21] N. Dalal, D. E. Holz, S. A. Hughes, and B. Jain, *Physical Review D* **74**, 063006 (2006).
- [22] S. Nissanke, D. E. Holz, N. Dalal, S. A. Hughes, J. L. Sievers, and C. M. Hirata, arXiv preprint arXiv:1307.2638 (2013).
- [23] S. Vitale and H.-Y. Chen, *Physical review letters* **121**, 021303 (2018).

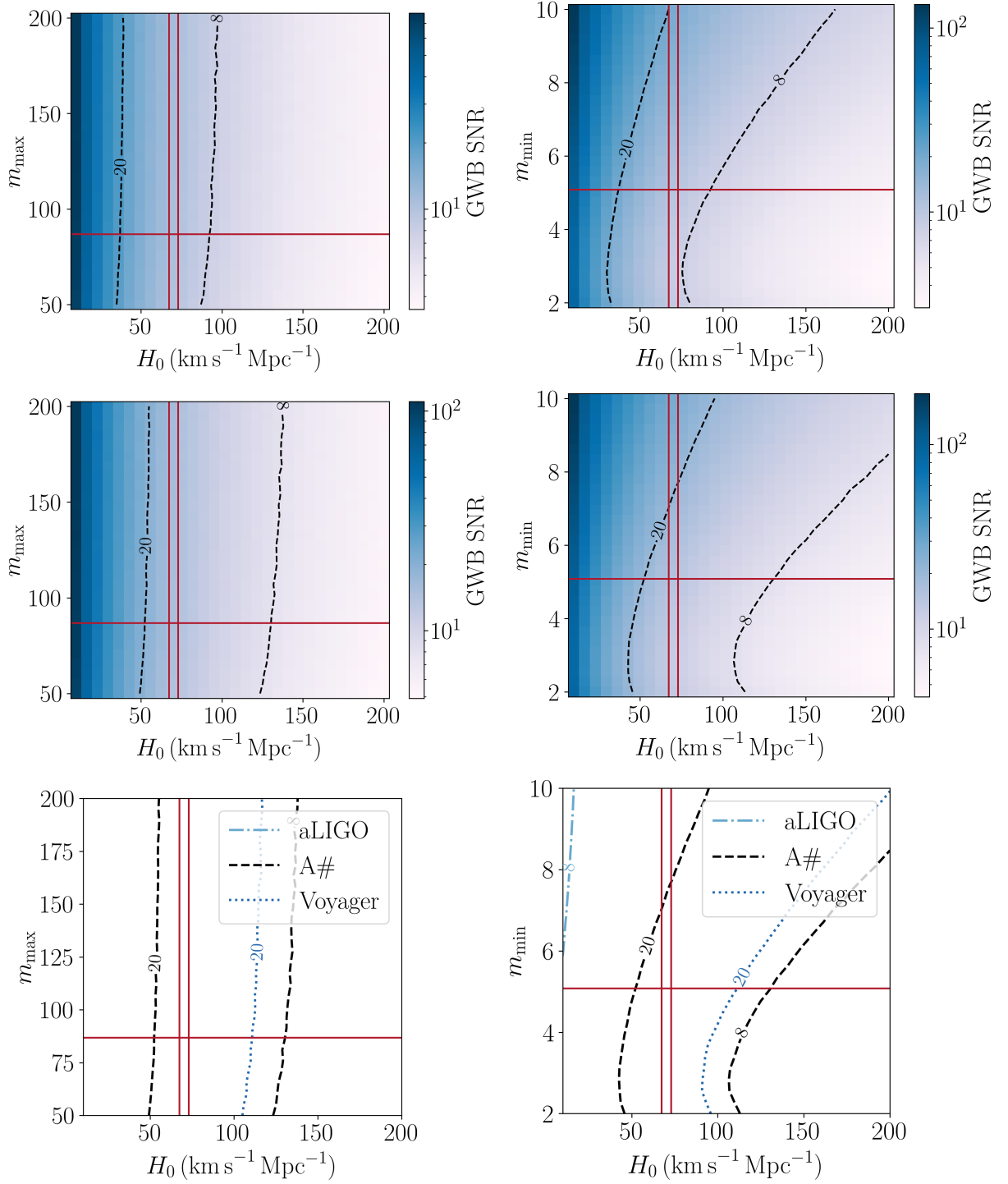


FIG. 9. SNR of the GWB for various future detector networks as a function of two parameters (H_0 with either m_{\max} or m_{\min}), with the other 13 (hyper)parameters fixed to values denoted in the text. Refer to Fig. 5 for more explanation of the subplots.

- [24] Abbott, B. P. *et al.*, *Nature* **551**, 85 (2017).
- [25] H.-Y. Chen, C.-J. Haster, S. Vitale, W. M. Farr, and M. Isi, *Monthly Notices of the Royal Astronomical Society* **513**, 2152 (2022).
- [26] I. Gupta, *Monthly Notices of the Royal Astronomical Society* **524**, 3537 (2023).
- [27] C. L. MacLeod and C. J. Hogan, *Physical Review D—Particles, Fields, Gravitation, and Cosmology* **77**, 043512 (2008).
- [28] W. Del Pozzo, *Physical Review D—Particles, Fields, Gravitation, and Cosmology* **86**, 043011 (2012).

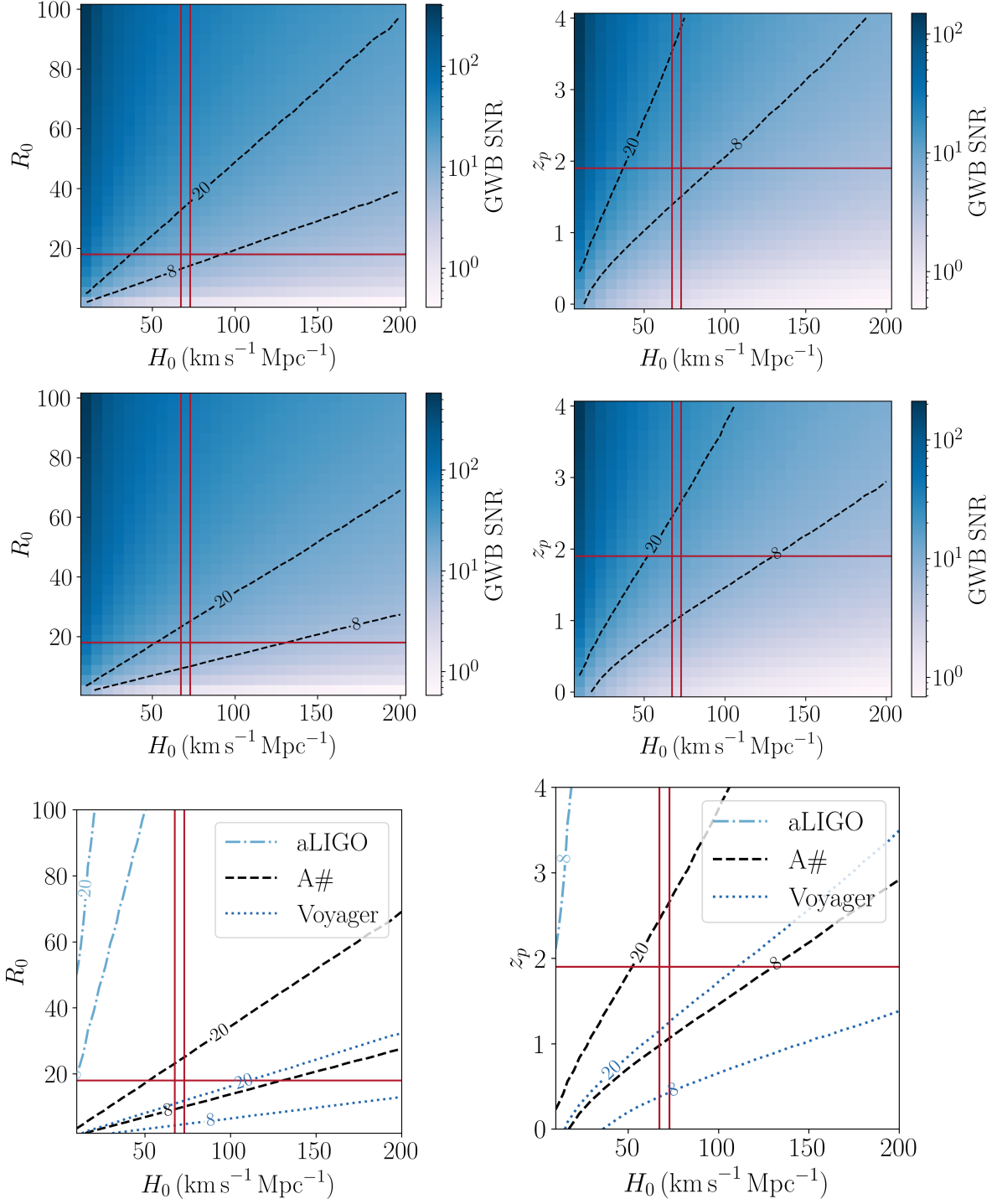


FIG. 10. SNR of the GWB for various future detector networks as a function of two parameters (H_0 with either R_0 or z_p), with the other 13 (hyper)parameters fixed to values denoted in the text. Refer to Fig. 5 for more explanation of the subplots.

- [29] A. Nishizawa, *Physical Review D* **96**, 101303 (2017).
- [30] H.-Y. Chen, M. Fishbach, and D. E. Holz, *Nature* **562**, 545 (2018).
- [31] R. Nair, S. Bose, and T. D. Saini, *Physical Review D* **98**, 023502 (2018).
- [32] M. Fishbach, R. Gray, I. M. Hernandez, H. Qi, A. Sur, F. Acernese, L. Aiello, A. Allocca, M. Aloy, A. Amato, *et al.*, *The Astrophysical Journal Letters* **871**, L13 (2019).
- [33] Soares-Santos, M. *et al.* (DES, LIGO Scientific, Virgo), *The Astrophysical Journal Letters* **876**, L7 (2019),

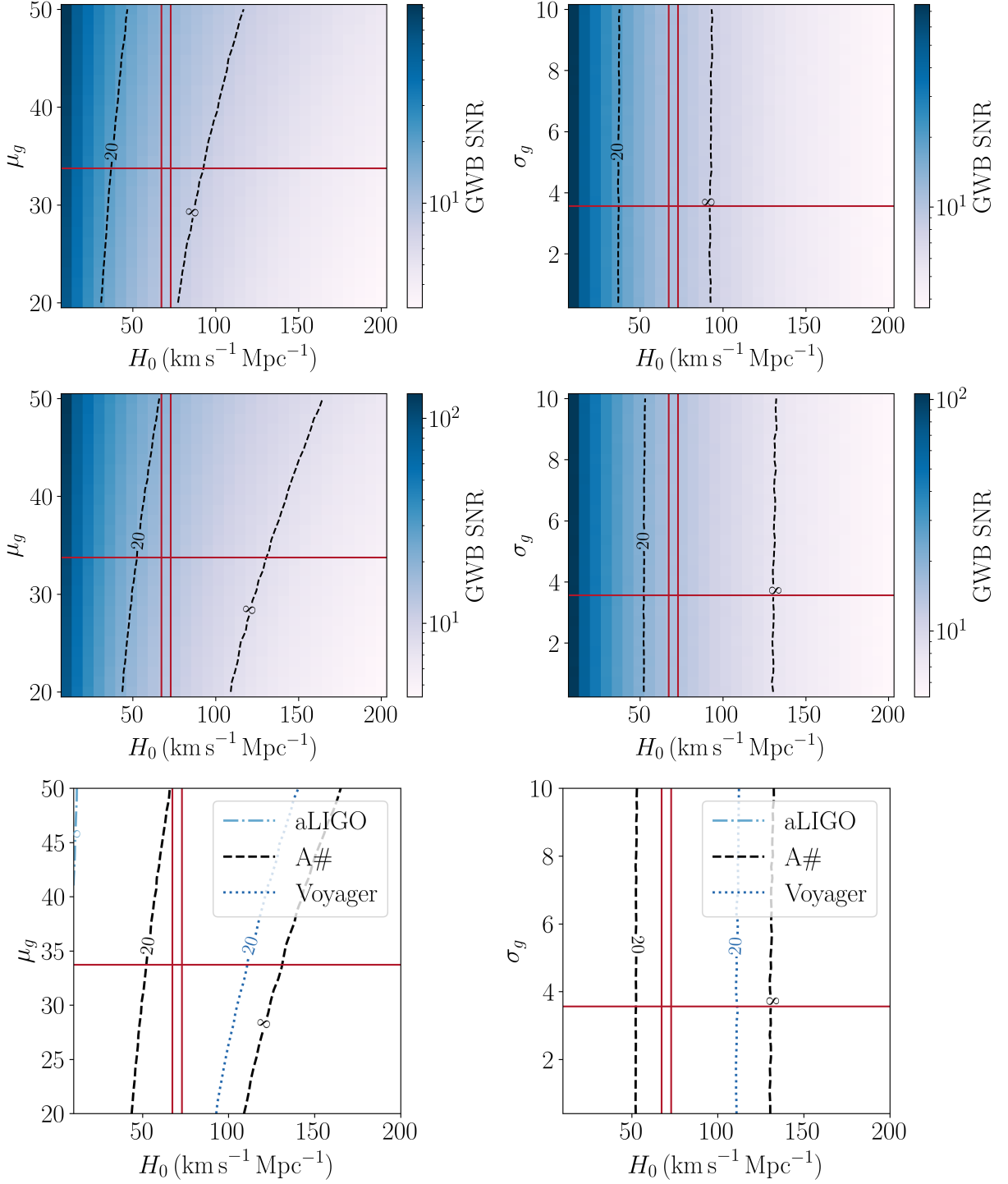


FIG. 11. SNR of the GWB for various future detector networks as a function of two parameters (H_0 with either μ_g or σ_g), with the other 13 (hyper)parameters fixed to values denoted in the text. Refer to Fig. 5 for more explanation of the subplots.

[arXiv:1901.01540](https://arxiv.org/abs/1901.01540) [astro-ph.CO].

- [34] R. Gray, I. M. Hernandez, H. Qi, A. Sur, P. R. Brady, H.-Y. Chen, W. M. Farr, M. Fishbach, J. R. Gair, A. Ghosh, *et al.*, *Physical Review D* **101**, 122001 (2020).
- [35] J. Yu, Y. Wang, W. Zhao, and Y. Lu, *Monthly Notices of the Royal Astronomical Society* **498**, 1786 (2020).
- [36] Palmese, Antonella *et al.*, *The Astrophysical Journal Letters* **900**, L33 (2020).
- [37] S. Borhanian, A. Dhani, A. Gupta, K. Arun, and B. Sathyaprakash, *The Astrophysical Journal Letters* **905**, L28 (2020).

- [38] A. Finke, S. Foffa, F. Iacovelli, M. Maggiore, and M. Mancarella, *Journal of Cosmology and Astroparticle Physics* **2021** (08), 026.
- [39] Abbott, R. and t. others (The LIGO Scientific Collaboration, *The Astrophysical Journal* **949**, 76 (2023).
- [40] Gray, Rachel *et al.*, *Journal of Cosmology and Astroparticle Physics* **2023** (12), 023.
- [41] C. Bom, V. Alfradique, A. Palmese, G. Teixeira, L. Santana-Silva, A. Santos, and P. Darc, *Monthly Notices of the Royal Astronomical Society* **535**, 961 (2024).
- [42] M. Oguri, *Physical Review D* **93**, 083511 (2016).
- [43] S. Bera, D. Rana, S. More, and S. Bose, *The Astrophysical Journal* **902**, 79 (2020).
- [44] S. Mukherjee, B. D. Wandelt, and J. Silk, *Monthly Notices of the Royal Astronomical Society* **494**, 1956 (2020).
- [45] S. Mukherjee, B. D. Wandelt, S. M. Nissanke, and A. Silvestri, *Physical Review D* **103**, 043520 (2021).
- [46] S. Mukherjee, A. Krolewski, B. D. Wandelt, and J. Silk, *The Astrophysical Journal* **975**, 189 (2024).
- [47] C. Messenger and J. Read, *Physical review letters* **108**, 091101 (2012).
- [48] D. Chatterjee, A. Hegade KR, G. Holder, D. E. Holz, S. Perkins, K. Yagi, and N. Yunes, *Physical Review D* **104**, 083528 (2021).
- [49] D. F. Chernoff and L. S. Finn, arXiv preprint gr-qc/9304020 (1993).
- [50] S. R. Taylor, J. R. Gair, and I. Mandel, *Physical Review D—Particles, Fields, Gravitation, and Cosmology* **85**, 023535 (2012).
- [51] S. R. Taylor and J. R. Gair, *Physical Review D—Particles, Fields, Gravitation, and Cosmology* **86**, 023502 (2012).
- [52] W. M. Farr, M. Fishbach, J. Ye, and D. E. Holz, *The Astrophysical Journal Letters* **883**, L42 (2019).
- [53] Z.-Q. You, X.-J. Zhu, G. Ashton, E. Thrane, and Z.-H. Zhu, *The Astrophysical Journal* **908**, 215 (2021).
- [54] J. M. Ezquiaga and D. E. Holz, *The Astrophysical Journal Letters* **909**, L23 (2021).
- [55] J. M. Ezquiaga and D. E. Holz, *Physical Review Letters* **129**, 061102 (2022).
- [56] U. Mali and R. Essick, *Astrophys. J.* **980**, 85 (2025), arXiv:2410.07416 [astro-ph.HE].
- [57] Abbott, B. P. *et al.* (LIGO Scientific, Virgo), *Phys. Rev. Lett.* **116**, 131102 (2016), arXiv:1602.03847 [gr-qc].
- [58] Abbott, R., others, and The LIGO Scientific Collaboration, Virgo Collaboration, and KAGRA Collaboration, *Physical Review D* **104**, 022004 (2021).
- [59] Abbott, R. *et al.* (LIGO, Virgo, and KAGRA Collaboration), *Phys. Rev. X* **13**, 011048 (2023), arXiv:2111.03634 [astro-ph.HE].
- [60] P. A. Rosado, *Physical Review D—Particles, Fields, Gravitation, and Cosmology* **84**, 084004 (2011).
- [61] X.-J. Zhu, E. Howell, T. Regimbau, D. Blair, and Z.-H. Zhu, *The Astrophysical Journal* **739**, 86 (2011).
- [62] S. Marassi, R. Schneider, G. Corvino, V. Ferrari, and S. P. Zwart, *Physical Review D—Particles, Fields, Gravitation, and Cosmology* **84**, 124037 (2011).
- [63] A. Starobinskii, *JETP Letters* **30**, 682 (1979).
- [64] T. W. Kibble, *Journal of Physics A: Mathematical and General* **9**, 1387 (1976).
- [65] R. Easther and E. A. Lim, *Journal of Cosmology and Astroparticle Physics* **2006** (04), 010.
- [66] C. Caprini and D. G. Figueroa, *Classical and Quantum Gravity* **35**, 163001 (2018).
- [67] G. Agazie, A. Anumarlapudi, A. M. Archibald, Z. Arzoumanian, P. T. Baker, B. Bécsy, L. Blecha, A. Brazier, P. R. Brook, S. Burke-Spolaor, *et al.*, *The Astrophysical Journal Letters* **951**, L8 (2023).
- [68] J. Antoniadis, P. Arumugam, S. Arumugam, S. Babak, M. Bagchi, A.-S. B. Nielsen, C. Bassa, A. Bathula, A. Berthereau, M. Bonetti, *et al.*, *Astronomy & Astrophysics* **678**, A50 (2023).
- [69] D. J. Reardon, A. Zic, R. M. Shannon, G. B. Hobbs, M. Bailes, V. Di Marco, A. Kapur, A. F. Rogers, E. Thrane, J. Askew, *et al.*, *The Astrophysical Journal Letters* **951**, L6 (2023).
- [70] H. Xu, S. Chen, Y. Guo, J. Jiang, B. Wang, J. Xu, Z. Xue, R. N. Caballero, J. Yuan, Y. Xu, *et al.*, *Research in Astronomy and Astrophysics* **23**, 075024 (2023).
- [71] T. Callister, M. Fishbach, D. E. Holz, and W. M. Farr, *The Astrophysical Journal* **896**, L32 (2020).
- [72] K. Turbang, M. Lalleman, T. A. Callister, and N. van Remortel, *The Astrophysical Journal* **967**, 142 (2024).
- [73] Abbott, Richard *et al.*, *Physical Review X* **13**, 041039 (2023).
- [74] Cousins, B. and Schumacher, K. and Chung, AKW and Talbot, C. and Callister, T. and Holz, D. and Yunes, N., Supplemental Material for “The Stochastic Siren: Astrophysical Gravitational-Wave Background Measurements of the Hubble Constant”, <https://doi.org/10.1103/41zh-bm7y> (2026).
- [75] B. Allen and J. D. Romano, *Physical Review D* **59**, 102001 (1999), arXiv:gr-qc/9710117.
- [76] V. Ferrari, S. Matarrese, and R. Schneider, *Monthly Notices of the Royal Astronomical Society* **303**, 258 (1999).
- [77] T. Regimbau and V. Mandic, *Classical and Quantum Gravity* **25**, 184018 (2008).
- [78] T. Regimbau, *Research in Astronomy and Astrophysics* **11**, 369 (2011).
- [79] J. D. Romano and N. J. Cornish, *Living Reviews in Relativity* **20**, 2 (2017), arXiv:1608.06889 [gr-qc].
- [80] D. W. Hogg, arXiv preprint astro-ph/9905116 (1999).
- [81] S. Dodelson and F. Schmidt, *Modern cosmology* (Elsevier, 2003).
- [82] S. R. Taylor and D. Gerosa, *Phys. Rev. D* **98**, 083017 (2018), arXiv:1806.08365 [astro-ph.HE].
- [83] I. Mandel, W. M. Farr, and J. R. Gair, *Mon. Not. Roy. Astron. Soc.* **486**, 1086 (2019), arXiv:1809.02063 [physics.data-an].
- [84] S. Vitale, D. Gerosa, W. M. Farr, and S. R. Taylor, *Handbook of Gravitational Wave Astronomy*, **1** (2022), arXiv:2007.05579 [astro-ph.IM].
- [85] W. M. Farr, *Research Notes of the AAS* **3**, 66 (2019).
- [86] R. Essick and M. Fishbach, *The Astrophysical Journal* **962**, 169 (2024).
- [87] Mastrogiovanni, Simone *et al.*, ICAROGW: A python package for inference of astrophysical population properties of noisy,

- heterogeneous and incomplete observations (2023), [arXiv:2305.17973 \[astro-ph, physics:gr-qc\]](#).
- [88] S. Drasco and É. É. Flanagan, *Phys. Rev. D* **67**, 082003 (2003), [arXiv:gr-qc/0210032 \[gr-qc\]](#).
- [89] R. Smith and E. Thrane, *Physical Review X* **8**, 021019 (2018), [arXiv:1712.00688 \[gr-qc\]](#).
- [90] V. Mandic, E. Thrane, S. Giampanis, and T. Regimbau, *Physical review letters* **109**, 171102 (2012).
- [91] T. Callister, A. S. Biscoveanu, N. Christensen, M. Isi, A. Matas, O. Minazzoli, T. Regimbau, M. Sakellariadou, J. Tasson, and E. Thrane, *Physical Review X* **7**, 041058 (2017).
- [92] N. Christensen, *Phys. Rev. D* **46**, 5250 (1992).
- [93] E. E. Flanagan, *Phys. Rev. D* **48**, 2389 (1993), [arXiv:astro-ph/9305029](#).
- [94] K. S. Thorne, *Three hundred years of gravitation*, 330 (1987).
- [95] P. Madau and M. Dickinson, *Annual Review of Astronomy and Astrophysics* **52**, 415 (2014), [arXiv:1403.0007 \[astro-ph.CO\]](#).
- [96] B. P. Abbott, others, and LIGO Scientific Collaboration and Virgo Collaboration, *The Astrophysical Journal* **882**, L24 (2019), [arXiv:1811.12940 \[astro-ph\]](#).
- [97] C. Talbot and E. Thrane, *Astrophys. J.* **856**, 173 (2018), [arXiv:1801.02699 \[astro-ph.HE\]](#).
- [98] C. Talbot, A. Farah, S. Galaudage, J. Golomb, and H. Tong, [arXiv preprint arXiv:2409.14143](#) (2024).
- [99] K. Belczynski, M. Dominik, T. Bulik, R. O’Shaughnessy, C. Fryer, and D. E. Holz, *The Astrophysical Journal Letters* **715**, L138 (2010).
- [100] D. Kushnir, M. Zaldarriaga, J. A. Kollmeier, and R. Waldman, *Monthly Notices of The Royal Astronomical Society* **462**, 844 (2016).
- [101] M. Gallegos-Garcia, C. P. Berry, P. Marchant, and V. Kalogera, *The Astrophysical Journal* **922**, 110 (2021).
- [102] L. Van Son, S. De Mink, T. Callister, S. Justham, M. Renzo, T. Wagg, F. Broekgaarden, F. Kummer, R. Pakmor, and I. Mandel, *The Astrophysical Journal* **931**, 17 (2022).
- [103] S. Rinaldi, W. Del Pozzo, M. Mapelli, A. Lorenzo-Medina, and T. Dent, *Astronomy & Astrophysics* **684**, A204 (2024).
- [104] S. Torniamenti, M. Mapelli, C. Périgois, M. A. Sedda, M. C. Artale, M. Dall’Amico, and M. P. Vaccaro, *Astronomy & Astrophysics* **688**, A148 (2024).
- [105] M. Lalleman, K. Turbang, T. Callister, and N. van Remortel, (2025), [arXiv:2501.10295 \[astro-ph.HE\]](#).
- [106] J. Skilling, *Bayesian inference and maximum entropy methods in science and engineering* **735**, 395 (2004).
- [107] J. Skilling, (2006).
- [108] J. S. Speagle, *Mon. Not. Roy. Astron. Soc.* **493**, 3132 (2020), [arXiv:1904.02180 \[astro-ph.IM\]](#).
- [109] G. Ashton *et al.*, *Astrophys. J. Suppl.* **241**, 27 (2019), [arXiv:1811.02042 \[astro-ph.IM\]](#).
- [110] V. Ferrari, S. Matarrese, and R. Schneider, *Mon. Not. Roy. Astron. Soc.* **303**, 247 (1999), [arXiv:astro-ph/9804259](#).
- [111] S. R. Chowdhury and M. Khlopov, *Phys. Rev. D* **110**, 063037 (2024), [arXiv:2409.01542 \[gr-qc\]](#).
- [112] S. Ferraiuolo, S. Mastrogiovanni, E. Kajfasz, and S. Escoffier, *in preparation*. (2025).
- [113] M. Fischbach, D. Davis, and A. Renzini, *Investigating data quality metrics for stochastic gravitational-wave detection* (2021).
- [114] Renzini, Arianna I *et al.*, *The Astrophysical Journal* **952**, 25 (2023).
- [115] A. I. Renzini and J. Golomb, [arXiv preprint arXiv:2407.03742](#) (2024).
- [116] Abbott, Benjamin P. *et al.* (LIGO Scientific, Virgo), *Phys. Rev. Lett.* **120**, 091101 (2018), [arXiv:1710.05837 \[gr-qc\]](#).
- [117] A. I. Renzini, B. Goncharov, A. C. Jenkins, and P. M. Meyers, *Stochastic Gravitational-Wave Backgrounds: Current Detection Efforts and Future Prospects* (2022), [arXiv:2202.00178 \[gr-qc\]](#).
- [118] P. Fritschel, K. Kuns, J. Driggers, A. Effler, B. Lantz, D. Ottaway, S. Ballmer, K. Dooley, R. Adhikari, M. Evans, B. Farr, G. Gonzalez, P. Schmidt, and S. Raja, *Report from the lsc post-o5 study group technical report t2200287 (ligo)* (2022).
- [119] Punturo, M *et al.*, *Classical and Quantum Gravity* **27**, 194002 (2010).
- [120] Reitze, David *et al.*, [arXiv preprint arXiv:1907.04833](#) [10.48550/arXiv.1907.04833](#) (2019).
- [121] Maggiore, Michele *et al.*, *Journal of Cosmology and Astroparticle Physics* **2020** (03), 050, 1912.02622.
- [122] Evans, Matthew *et al.* [10.48550/arXiv.2109.09882](#) (2021), [2109.09882](#).
- [123] Evans, Matthew *et al.*, (2023), [arXiv:2306.13745 \[astro-ph.IM\]](#).
- [124] Branchesi, Marica *et al.*, *JCAP* **07**, 068, [arXiv:2303.15923 \[gr-qc\]](#).
- [125] R. Busicchio, A. Ain, M. Ballelli, G. Cella, and B. Patricelli, *Phys. Rev. D* **107**, 063027 (2023), [arXiv:2209.01400 \[gr-qc\]](#).
- [126] Astropy Collaboration *et al.*, *Astronomy and Astrophysics* **558**, A33 (2013), [arXiv:1307.6212 \[astro-ph.IM\]](#).
- [127] Astropy Collaboration and others (Astropy Contributors), *The Astronomical Journal* **156**, 123 (2018), [arXiv:1801.02634 \[astro-ph.IM\]](#).
- [128] Astropy Collaboration *et al.*, *Astrophys. J.* **935**, 167 (2022), [arXiv:2206.14220 \[astro-ph.IM\]](#).
- [129] A. Collette, *Python and HDF5: unlocking scientific data* (“ O’Reilly Media, Inc.”, 2013).
- [130] J. D. Hunter, *Computing in science & engineering* **9**, 90 (2007).
- [131] Harris, Charles R *et al.*, *Nature* **585**, 357 (2020).
- [132] Virtanen, Pauli *et al.*, *Nature methods* **17**, 261 (2020).
- [133] A. I. Renzini and J. Golomb, *Astronomy & Astrophysics* **691**, A238 (2024).
- [134] D. Meacher, M. Coughlin, S. Morris, T. Regimbau, N. Christensen, S. Kandhasamy, V. Mandic, J. D. Romano, and E. Thrane, *Physical Review D* **92**, 063002 (2015).
- [135] S. E. Perkins, R. Nair, H. O. Silva, and N. Yunes, *Physical Review D* **104**, 024060 (2021).
- [136] E. V. Linder, *Physical Review Letters* **90**, 091301 (2003), [arXiv:astro-ph/0208512](#).
- [137] X.-J. Zhu, E. J. Howell, D. G. Blair, and Z.-H. Zhu, *Monthly Notices of the Royal Astronomical Society* **431**, 882 (2013),

[arXiv:1209.0595](#) [astro-ph, physics:gr-qc].

- [138] N. Christensen and R. Meyer, *Reviews of Modern Physics* **94**, 025001 (2022), [arXiv:2204.04449](#) [gr-qc].
- [139] C. Pérois, C. Belczynski, T. Bulik, and T. Regimbau, *Physical Review D* **103**, 043002 (2021).
- [140] Abbott, Benjamin P. *et al.* (LIGO Scientific, Virgo), *Phys. Rev. Lett.* **120**, 091101 (2018), [arXiv:1710.05837](#) [gr-qc].
- [141] É. É. Flanagan and S. A. Hughes, *Physical Review D* **57**, 4535 (1998).
- [142] C. Wu, V. Mandic, and T. Regimbau, *Physical Review D—Particles, Fields, Gravitation, and Cosmology* **85**, 104024 (2012).
- [143] Adhikari, R X *et al.*, *Classical and Quantum Gravity* **37**, 165003 (2020).
- [144] Ade, Peter AR *et al.*, *Astronomy & Astrophysics* **594**, A13 (2016).
- [145] https://docs.scipy.org/doc/scipy/reference/generated/scipy.stats.gaussian_kde.html.